

Efficient slave-boson approach for multiorbital two-particle response functions and superconductivity

Tsung-Han Lee¹, Nicola Lanatà^{2,3}, Minjae Kim^{1,4}, Gabriel Kotliar^{1,5}

¹*Physics and Astronomy Department, Rutgers University, Piscataway, New Jersey 08854, USA*

²*Department of Physics and Astronomy, Aarhus University, 8000 Aarhus C, Denmark*

³*Nordita, KTH Royal Institute of Technology and Stockholm University,
Hannes Alfvéns väg 12, SE-106 91 Stockholm, Sweden*

⁴*Department of Chemistry, Pohang University of Science and Technology (POSTECH), Pohang 37673, Korea and*

⁵*Condensed Matter Physics and Materials Science Department,
Brookhaven National Laboratory, Upton, New York 11973, USA*

We develop an efficient approach for computing two-particle response functions and interaction vertices for multiorbital strongly correlated systems based on the rotationally-invariant slave-boson framework. The method is applied to the degenerate three-orbital Hubbard-Kanamori model for investigating the origin of the s -wave orbital antisymmetric spin-triplet superconductivity in the Hund's metal regime, previously found in the dynamical mean-field theory studies. By computing the pairing interaction considering the particle-particle and the particle-hole scattering channels, we identify the mechanism leading to the pairing instability around Hund's metal crossover arises from the particle-particle channel, containing the local electron pair fluctuation between different particle-number sectors of the atomic Hilbert space. On the other hand, the particle-hole spin fluctuations induce the s -wave pairing instability before entering the Hund's regime. Our approach paves the way for investigating the pairing mechanism in realistic correlated materials.

I. INTRODUCTION

Slave-boson approaches are among the most widely used theories for describing strongly correlated systems [1–7]. In particular, the saddle-point approximation of the slave-boson method provides a reliable description of the local correlation effects, while requiring a relatively low computational cost compared to dynamical mean-field theory (DMFT) [8]. The development of the rotationally-invariant slave-boson (RISB) saddle-point approximation [9], equivalent to the Gutzwiller approximation (GA) [10, 11], has also been extended to realistic multiorbital systems, in combination with density functional theory [12, 13], uncovering many intriguing phenomena, including selective-Mott transition [7, 14, 15], Hund's metal behavior [16–19], valence fluctuations, and correlation induced topological materials [20–22].

Recently, RISB has been reformulated as a quantum embedding theory, where the interacting lattice problem is mapped to an impurity problem coupled to a self-consistently determined environment [21], similar to DMFT and density matrix embedding theory (DMET) [8, 23, 24]. In particular, the RISB saddle-point equations are equivalent to the “non-interacting bath” DMET (NIB-DMET) self-consistent equations when setting the quasiparticle renormalization matrix to unity and enforcing an additional constraint on the structure of the physical density matrix [25, 26]. In addition, the two methods, originally proposed for describing the ground state or low-temperature properties, have been extended to study the finite-temperature effects, the non-equilibrium dynamics, the excited states, and the single-particle spectral functions in correlated systems [27–33].

So far, RISB is mostly used for investigating the single-particle spectral functions and the static local observ-

ables. However, the two-particle response functions and the corresponding interaction vertices are also important for explaining the emergent phenomena in correlated materials, e.g., the spin-fluctuation mediated pairing in unconventional superconductors [34]. It is, therefore, important to extend RISB to study these quantities. Indeed, it is possible to compute the two-particle response functions with the Gaussian fluctuation approach around the slave-boson saddle-point [3, 4, 35–44]. However, the technique is so far restricted to the single-orbital Hubbard model. On the other hand, the development of the time-dependent Gutzwiller approximation has been extended to multiorbital systems and applied to the two-orbital Hubbard model for spin susceptibilities [45–51]. To the best of our knowledge, the theories have not been generalized to compute arbitrary two-particle response functions and quasiparticle interaction vertices for multiorbital systems.

In this work, we develop an efficient approach to compute general susceptibilities and quasiparticle interaction vertices based on fluctuation around the RISB saddle-point, allowing a diagrammatic analysis for the pairing mechanism. We apply our method to the degenerate three-orbital Hubbard-Kanamori model to investigate the origin of the s -wave orbital-antisymmetric spin-triplet pairing instability in the Hund's metal regime, previously found in the DMFT and GA studies [52–55]. We show that, in agreement with DMFT [53], our approach captures the s -wave spin-triplet pairing instability around the Hund's metal crossover. By investigating the pairing interaction considering the particle-particle and the particle-hole scattering channel, we identify that the mechanism leading to the local s -wave orbital-antisymmetric spin-triplet pairing arises from the particle-particle channel, containing the local electron

pair fluctuation between different particle-number sectors of the local Hilbert space. Interestingly, the particle-hole spin-fluctuation mechanism for the s -wave pairing, considered also in previous works [53, 56, 57], induces the s -wave pairing instability slightly before entering the Hund's regime. Possible applications of our formalism to NIB-DMET are also discussed.

II. MODEL

We consider the following generic multi-orbital Hubbard-Kanamori model:

$$\hat{H} = \sum_{\mathbf{k}\alpha\beta\sigma} \epsilon_{\mathbf{k}\alpha\beta} d_{\mathbf{k}\alpha\sigma}^\dagger d_{\mathbf{k}\beta\sigma} + \sum_i \hat{H}_{\text{loc}}[\{d_{i\alpha\sigma}^\dagger, d_{i\alpha\sigma}\}], \quad (1)$$

where α is the orbital index, σ is the spin index, i is the unit-cell label, and \mathbf{k} is the momentum conjugate to i . As a proof of principle and for pedagogical reason, we will assume a three-orbital degenerate model with the energy dispersion of a two-dimensional square lattice with the nearest neighbor hopping:

$$\epsilon_{\mathbf{k}\alpha\beta} = -2t(\cos(\mathbf{k}_x) + \cos(\mathbf{k}_y))\delta_{\alpha,\beta}, \quad (2)$$

where $\alpha \in \{1, 2, 3\}$, and we will set $t = 1$ as the energy unit. However, we note that our formalism applies to multiorbital Hubbard models with general hopping matrix and arbitrary number of orbitals. The term H_{loc} represents the following operator:

$$\begin{aligned} \hat{H}_{\text{loc}}[\{d_{i\alpha}^\dagger, d_{i\alpha}\}] &= U \sum_{\alpha} n_{i\alpha\uparrow} n_{i\alpha\downarrow} + U' \sum_{\alpha < \alpha', \sigma} n_{i\alpha\sigma} n_{i\alpha'\sigma} \\ &+ (U' - J) \sum_{\alpha < \alpha', \sigma} n_{i\alpha\sigma} n_{i\alpha'\sigma} - J \sum_{\alpha < \alpha'} (d_{i\alpha\uparrow}^\dagger d_{i\alpha\downarrow} d_{i\alpha'\downarrow}^\dagger d_{i\alpha'\uparrow} \\ &+ d_{i\alpha\uparrow}^\dagger d_{i\alpha\downarrow}^\dagger d_{i\alpha'\uparrow} d_{i\alpha'\downarrow} + \text{H.c.}) - \mu_0 \sum_{\alpha\sigma} n_{\alpha\sigma}, \end{aligned} \quad (3)$$

which contains the Kanamori interaction [58] in the cubic-harmonic basis. The first term is the intra-orbital Coulomb interaction, the second term and the third term is the inter-orbital Coulomb interaction, and the last term contains the spin-flip and the pairing hopping interaction. Throughout our paper, we assume the rotationally invariant condition $U' = U - 2J$ and set $J = U/4$. Note that, with this choice of parameters, the bare orbital-antisymmetric spin-triplet pairing interaction is repulsive, i.e., $U' - J > 0$. The electron occupancy is controlled by the chemical potential μ_0 .

Due to the $O(3) \otimes SU(2)$ symmetry in the degenerate three-orbital model, the orbital-antisymmetric spin-triplet pairing channels [59–61] are related to each other by a rotation in the orbital and the spin space. Consequently, we focus on the pairing fluctuation in one of the orbital-antisymmetric spin-triplet pairing channels:

$$\hat{O}_{\text{P}} = \sum_{\alpha\beta} \sum_{\sigma\sigma'} [\lambda_6]_{\alpha\beta} [-i\sigma_y \sigma_z]_{\sigma\sigma'} d_{i,\alpha\sigma}^\dagger d_{i,\beta\sigma'}^\dagger. \quad (4)$$

Similarly, we have the following independent operators for the charge, spin, orbital, and spin-orbital fluctuation channels:

$$\hat{O}_s = \begin{cases} \sum_{\alpha\beta} [\lambda_0]_{\alpha\beta} [\sigma_0]_{\sigma\sigma'} d_{i,\alpha\sigma}^\dagger d_{i,\beta\sigma'} & s = \text{ch} \\ \sum_{\alpha\beta} [\lambda_0]_{\alpha\beta} [\sigma_z]_{\sigma\sigma'} d_{i,\alpha\sigma}^\dagger d_{i,\beta\sigma'} & s = \text{sp} \\ \sum_{\alpha\beta} [\lambda_4]_{\alpha\beta} [\sigma_0]_{\sigma\sigma'} d_{i,\alpha\sigma}^\dagger d_{i,\beta\sigma'} & s = \text{orb} \\ \sum_{\alpha\beta} [\lambda_4]_{\alpha\beta} [\sigma_z]_{\sigma\sigma'} d_{i,\alpha\sigma}^\dagger d_{i,\beta\sigma'} & s = \text{so} \\ \sum_{\alpha\beta} [\lambda_1]_{\alpha\beta} [\sigma_0]_{\sigma\sigma'} d_{i,\alpha\sigma}^\dagger d_{i,\beta\sigma'} & s = \text{orb}^* \\ \sum_{\alpha\beta} [\lambda_1]_{\alpha\beta} [\sigma_z]_{\sigma\sigma'} d_{i,\alpha\sigma}^\dagger d_{i,\beta\sigma'} & s = \text{so}^*, \end{cases} \quad (5)$$

where we label the fluctuation channels by $s \in \{\text{ch}, \text{sp}, \text{orb}, \text{so}, \text{orb}^*, \text{so}^*, \text{P}\}$ throughout the paper. Here, λ_0 is the 3×3 identity matrix and λ_i are the Gell-Mann matrices (see Appx. A), while σ_0 is the 2×2 identity matrix and σ_i ($i = x, y, z$) are the Pauli matrices.

III. METHOD

Our fluctuation approach around the RISB normal-state saddle-point is entirely encoded in the following Lagrange function [62] (see Appx. (B)):

$$\mathcal{L}[\langle\Phi\rangle, \mathbf{R}, \mathbf{\Lambda}; \mathbf{D}, \mathbf{\Lambda}^c, E^c, \mathbf{\Delta}] = \mathcal{L}_{\text{qp}}[\mathbf{R}, \mathbf{\Lambda}] + \mathcal{L}_{\text{emb}}[\mathbf{D}, \mathbf{\Lambda}^c, \langle\Phi\rangle, E^c] + \mathcal{L}_{\text{mix}}[\mathbf{D}, \mathbf{R}, \mathbf{\Lambda}^c], \quad (6)$$

where:

$$\mathcal{L}_{\text{qp}}[\mathbf{R}, \mathbf{\Lambda}] = \frac{-T}{N} \frac{1}{2} \sum_{\mathbf{k}_1 \mathbf{k}_2 \omega_n} \text{Tr} \log \left[-i\omega_n + H_{\mathbf{k}_1 \mathbf{k}_2}^{\text{qp}} \right] e^{i\omega_n 0^+} \quad (7)$$

$$\begin{aligned} \mathcal{L}_{\text{emb}}[\mathbf{D}, \mathbf{\Lambda}^c, \langle\Phi\rangle, E^c] &= \sum_i \langle\Phi_i | \hat{H}_{i,\text{emb}}[\mathbf{D}_i, \mathbf{\Lambda}_i^c] | \Phi_i \rangle \\ &+ E_i^c (\langle\Phi_i | \Phi_i \rangle - 1) \end{aligned} \quad (8)$$

$$\begin{aligned} \mathcal{L}_{\text{mix}}[\mathbf{D}, \mathbf{R}, \mathbf{\Lambda}^c] &= - \sum_i \left[\frac{1}{2} \sum_{ab} ([\mathbf{\Lambda}_i]_{ab} + [\mathbf{\Lambda}_i^c]_{ab}) [\mathbf{\Delta}_i]_{ab} \right. \\ &\left. + \sum_{a\alpha} ([\mathbf{D}_i]_{a\alpha} [\mathbf{R}_i]_{c\alpha} [\mathbf{\Delta}_i (1 - \mathbf{\Delta}_i)]_{ca}^{1/2} + \text{c.c.}) \right]. \end{aligned} \quad (9)$$

Equation (7) encodes the contribution of the so-called ‘‘quasiparticle fermionic’’ degrees of freedom. Specifically, the matrix:

$$[H_{\mathbf{k}_1 \mathbf{k}_2}^{\text{qp}}]_{ab} = \frac{1}{N} \sum_{\mathbf{k}} [\mathbf{R}_{\mathbf{k}_1 - \mathbf{k}} \tilde{\epsilon}_{\mathbf{k}} \mathbf{R}_{\mathbf{k}_2 - \mathbf{k}}^\dagger]_{ab} + [\mathbf{\Lambda}_{\mathbf{k}_1 - \mathbf{k}_2}]_{ab}, \quad (10)$$

with the hopping term in the Nambu basis

$$\tilde{\epsilon}_{\mathbf{k}} = \begin{pmatrix} \epsilon_{\mathbf{k}} & 0 \\ 0 & -\epsilon_{-\mathbf{k}}^* \end{pmatrix}, \quad (11)$$

characterizes the ‘‘quasiparticle Hamiltonian’’:

$$\hat{H}^{\text{qp}} = \sum_{\mathbf{k}_1, \mathbf{k}_2} [H_{\mathbf{k}_1 \mathbf{k}_2}^{\text{qp}}]_{ab} \Psi_{\mathbf{k}_1 a}^\dagger \Psi_{\mathbf{k}_2 b}, \quad (12)$$

where $\Psi_{\mathbf{k}}^\dagger = (f_{\mathbf{k}1\uparrow}^\dagger f_{\mathbf{k}1\downarrow}^\dagger \dots f_{\mathbf{k}M\uparrow}^\dagger f_{\mathbf{k}M\downarrow}^\dagger f_{\mathbf{k}1\uparrow} f_{\mathbf{k}1\downarrow} \dots f_{\mathbf{k}M\uparrow} f_{\mathbf{k}M\downarrow})$ is a Nambu spinor, $f_{\mathbf{k}\alpha\sigma}$ are the fermionic quasiparticle modes, and M is the total number of orbitals. The matrix \mathbf{R} is the so-called ‘‘quasiparticle renormalization matrix’’ and $\mathbf{\Lambda}$ is a matrix of Lagrange multipliers enforcing the RISB constraints [9, 62]:

$$[\mathbf{\Lambda}_i]_{ab} \equiv \langle \Psi_{ia}^\dagger \Psi_{ib} \rangle_T, \quad (13)$$

where $\mathbf{\Delta}_i$ corresponds to the local quasiparticle density matrices [14], and the symbol $\langle \dots \rangle_T$ denotes the thermal average of the non-interacting quasiparticle Hamiltonian \hat{H}^{qp} at temperature T .

The second term \mathcal{L}_{emb} (Eq. (8)) encodes the contribution of the slave-boson amplitudes, that here we expressed directly in terms of the corresponding ‘‘quantum embedding’’ states $|\Phi_i\rangle$ and *interacting* embedding Hamiltonians [21] (see Appx. B 1):

$$\begin{aligned} \hat{H}_{i,\text{emb}} = & H_{i,\text{loc}}[\{\hat{d}_{i\alpha}^\dagger, \hat{d}_{i\alpha}\}] + \left(\sum_{\alpha\alpha\beta} \mathbf{D}_{i\alpha\alpha} \hat{\Xi}_{i\alpha}^\dagger \hat{\Psi}_{i\beta} \bar{I}_{ba} + \text{H.c.} \right) \\ & + \sum_{abcd} \frac{1}{2} \mathbf{\Lambda}_{iab}^c \bar{I}_{bc} \hat{\Psi}_{ic}^\dagger \hat{\Psi}_{id} \bar{I}_{da}, \end{aligned} \quad (14)$$

where $\hat{\Xi}_i^\dagger = (\hat{d}_{i1\uparrow}^\dagger \hat{d}_{i1\downarrow}^\dagger \dots \hat{d}_{iM\uparrow}^\dagger \hat{d}_{iM\downarrow}^\dagger \hat{d}_{i1\uparrow} \hat{d}_{i1\downarrow} \dots \hat{d}_{iM\uparrow} \hat{d}_{iM\downarrow})$ is the impurity Nambu spinor and $\hat{\Psi}_i^\dagger = (f_{i1\uparrow}^\dagger f_{i1\downarrow}^\dagger \dots f_{iM\uparrow}^\dagger f_{iM\downarrow}^\dagger f_{i1\uparrow} f_{i1\downarrow} \dots f_{iM\uparrow} f_{iM\downarrow})$ is the Nambu spinor for the bath orbitals. The matrix

$$\bar{I} = \begin{pmatrix} \mathbf{1} & 0 \\ 0 & -\mathbf{1} \end{pmatrix} \quad (15)$$

is the sign exchange matrix generated from the embedding mapping (see Appx. B 1), where $\mathbf{1}$ is the $2M \times 2M$ identity matrix. The variable E_i^c is a Lagrange multiplier enforcing the normalization of $|\Phi_i\rangle$:

$$\langle \Phi_i | \Phi_i \rangle \equiv 1. \quad (16)$$

The matrix $\mathbf{\Lambda}_i^c$, describing the embedding Hamiltonian bath potential, is a matrix of Lagrange multipliers enforcing the RISB constraints:

$$[\mathbf{\Lambda}_i]_{ab} \equiv \langle \Phi_i | \hat{\Psi}_{ib} \hat{\Psi}_{ia}^\dagger | \Phi_i \rangle. \quad (17)$$

The matrix \mathbf{D}_i , describing the hybridization between the impurity and the bath orbitals, is a matrix of Lagrange

multipliers, enforcing the definition of the renormalization matrix [9, 14, 62]

$$\mathbf{R}_{i\alpha\alpha} = \sum_b \langle \Phi_i | \hat{\Xi}_{i\alpha}^\dagger \hat{\Psi}_{ib} | \Phi_i \rangle [\mathbf{\Delta}_i (1 - \mathbf{\Delta}_i)]_{ba}^{-\frac{1}{2}}. \quad (18)$$

The third term \mathcal{L}_{mix} (Eq. (9)) contains the Lagrange multipliers from both \mathcal{L}_{qp} and \mathcal{L}_{emb} .

All physical observables can be obtained from the above variational variables at the saddle-point solution of Eq. (6). The total energy is equal to the Lagrange function (Eq. (6)) evaluated at the saddle-point. The expectation value of generic local operators $\hat{\mathcal{O}}_i[\{d_{i\alpha}, d_{i\alpha}^\dagger\}]$ is determined from:

$$\langle \hat{\mathcal{O}}_i[\{d_{i\alpha}, d_{i\alpha}^\dagger\}] \rangle \equiv \langle \Phi_i | \hat{\mathcal{O}}_i[\{\hat{d}_{i\alpha}, \hat{d}_{i\alpha}^\dagger\}] | \Phi_i \rangle. \quad (19)$$

In particular, the local (physical) single-particle density matrix is obtained from:

$$\rho_{i,\alpha\beta} \equiv \langle \Phi_i | \hat{\Xi}_{i\alpha}^\dagger \hat{\Xi}_{i\beta} | \Phi_i \rangle, \quad (20)$$

The quasiparticle weight is determined from the \mathbf{R} matrix through $Z_i = \mathbf{R}_i^\dagger \mathbf{R}_i$.

Note that within the context of NIB-DMET, Eq. (12) corresponds to the so-called ‘‘low-level mean-field’’ Hamiltonian when setting $\mathbf{R} = I$, and $\mathbf{\Lambda}$ is termed ‘‘correlation potential’’. Equation (14) corresponds to the so-called ‘‘high-level many-body Hamiltonian’’ in NIB-DMET, where the two-particle interaction on the bath orbitals is set to zero [24].

A. Parameterization of the single-particle matrices

To enforce the symmetry conditions of the Lagrange function, we introduce the following parameterization of the renormalization matrix, \mathbf{R}_i , and the Lagrange multipliers, $\mathbf{\Lambda}_i$, $\mathbf{\Delta}_i$, \mathbf{D}_i , and $\mathbf{\Lambda}_i^c$ [14]:

$$\mathbf{R}_i = \sum_s r_{i,s} \tilde{\mathbf{h}}_s, \quad (21)$$

$$\mathbf{\Lambda}_i = \sum_s l_{i,s} \mathbf{h}_s, \quad (22)$$

$$\mathbf{\Delta}_i = \frac{1}{2} \mathbf{1} + \sum_s d_{i,s} \mathbf{h}_s^t, \quad (23)$$

$$\mathbf{D}_i = \sum_s D_{i,s} \tilde{\mathbf{h}}_s, \quad (24)$$

$$\mathbf{\Lambda}_i^c = \sum_s l_{i,s}^c \mathbf{h}_s, \quad (25)$$

where $\mathbf{1}$ is the $4M \times 4M$ identity matrix, and \mathbf{h}_s and $\tilde{\mathbf{h}}_s$ are the symmetry-adapted matrix basis of the above single-particle matrices. The structure of the matrix basis \mathbf{h}_s and $\tilde{\mathbf{h}}_s$ is determined from the group symmetry analysis of the model in the presence of the fluctuating operators (e.g., Eqs. (4)-(5)) [14]. This parameterization

allows us to classify the fluctuations of the variational parameters (r_s , l_s , etc.) to a specific symmetry channel s , associated to \mathbf{h}_s and $\tilde{\mathbf{h}}_s$. For example, in the degenerate three-orbital Hubbard-Kanamori model, the \mathbf{h}_s and $\tilde{\mathbf{h}}_s$ (see Appx. C 2) are associated to the fluctuation channels $s \in \{\text{ch, sp, orb, so, orb}^*, \text{so}^*, \text{P}\}$ in Eqs. (4)-(5). In addition, for computing the susceptibility of a given channel s , the embedding wavefunction $|\Phi_i\rangle$ has to break the corresponding symmetry, e.g., the particle number conservation of $|\Phi_i\rangle$ has to be broken for the pairing susceptibility calculations.

For later convenience, we introduce the following vector of parameters:

$$\mathbf{x}_i = (r_{i,\text{ch}}, l_{i,\text{ch}}, d_{i,\text{ch}}, D_{i,\text{ch}}, l_{i,\text{ch}}^c, \dots, r_{i,s}, l_{i,s}, d_{i,s}, D_{i,s}, l_{i,s}^c, \dots, r_{i,\text{P}}, l_{i,\text{P}}, d_{i,\text{P}}, D_{i,\text{P}}, l_{i,\text{P}}^c), \quad (26)$$

and assume that all of its entries are real, which is sufficient for static quantities (e.g., static susceptibilities and Landau parameters [39, 42]). Note that our assumption of real variables is applicable for our model without spin-orbit coupling. The generalization to spin-orbit coupled systems can be straightforwardly obtained using the same procedure proposed in this work, by including in the Lagrangian also the imaginary part of \mathbf{R} and \mathbf{D} .

B. Saddle-point approximation

The first step of our fluctuation approach is to determine the normal-state saddle-point solution without any ordering. We assume a spatially homogeneous saddle-point solution, where \mathbf{x}_i does not depend on i .

Performing the partial derivatives of Eq. (48) with respect to \mathbf{x} , we arrive the following saddle-point equations:

$$[\Delta]_{ab} = \frac{1}{N} \sum_{\mathbf{k}} [f_T(H_{\mathbf{k}}^{\text{qp}})]_{ba}, \quad (27)$$

$$[\Delta(1 - \Delta)]_{ac}^{1/2} \mathbf{D}_{ca} = \frac{1}{N} \frac{1}{2} \sum_{\mathbf{k}} [\tilde{\epsilon}_{\mathbf{k}} R^\dagger f_T(H_{\mathbf{k}}^{\text{qp}})]_{\alpha\alpha}, \quad (28)$$

$$\sum_{cb\alpha} \partial_{d_s} [\Delta(1 - \Delta)]_{cb}^{1/2} [\mathbf{D}]_{b\alpha} [\mathbf{R}]_{c\alpha} + \text{c.c.} + \frac{1}{2} [l_s + l_s^c] = 0, \quad (29)$$

$$\hat{H}_{\text{emb}} |\Phi\rangle = E^c |\Phi\rangle, \quad (30)$$

$$[\mathcal{F}^{(1)}]_{ab} \equiv \langle \Phi | \bar{I}_{bc} \hat{\Psi}_c \hat{\Psi}_d^\dagger \bar{I}_{da} | \Phi \rangle - [\Delta]_{ab} = 0, \quad (31)$$

$$[\mathcal{F}^{(2)}]_{\alpha\alpha} \equiv \langle \Phi | \hat{\Xi}_\alpha^\dagger \hat{\Psi}_b \bar{I}_{ba} | \Phi \rangle - \mathbf{R}_{c\alpha} [\Delta(1 - \Delta)]_{ca}^{1/2} = 0, \quad (32)$$

where f_T is the Fermi function and $H_{\mathbf{k}}^{\text{qp}} = \mathbf{R} \tilde{\epsilon}_{\mathbf{k}} \mathbf{R}^\dagger + \mathbf{\Lambda}$ is the saddle-point quasiparticle Hamiltonian. Equations (27)-(32) can be solved numerically utilizing quasi-Newton methods [14, 21]. Note that our saddle-point equations yield consistent results compared to the formalism in Ref. [62].

It is also interesting to point out that Eqs. (27)-(32) are equivalent to the NIB-DMET self-consistent equations when setting the renormalization matrix to unity $\mathbf{R} = I$ and enforcing the so-called ‘‘quasiparticle constraint’’ that we will introduce later in Sec. IV [25].

Given the saddle-point solution in the normal phase, we want to compute the corresponding susceptibilities. This will be accomplished using the approach described below.

C. Calculation of susceptibilities

Here we describe the formalism for calculating the susceptibilities in multi-orbital systems within the RISB framework. For concreteness, we focus on uniform susceptibilities in this section, where \mathbf{x}_i is independent of i and we suppress the i index in the following derivation. The generalization to susceptibilities with finite momentum transfer is described in Sec. IV.

Let us consider the RISB Lagrange function (Eq. (6)) in the presence of a local perturbation, proportional to a generic operator \hat{O} :

$$\mathcal{L}[\xi, \mathbf{x}, \Phi, E^c] = \mathcal{L}_{\text{qp}}[\mathbf{x}] + \mathcal{L}_{\text{mix}}[\mathbf{x}] + \mathcal{L}_{\text{emb}}[\xi, \mathbf{x}, \Phi, E^c], \quad (33)$$

where we have modified the embedding part of the Lagrangian to

$$\mathcal{L}_{\text{emb}}[\xi, \mathbf{x}, \Phi, E^c] = \sum_i \langle \Phi(\mathbf{x}) | \hat{H}_{\text{emb}}[\mathbf{x}] - \xi \hat{O} | \Phi(\mathbf{x}) \rangle + E^c (1 - \langle \Phi(\mathbf{x}) | \Phi(\mathbf{x}) \rangle), \quad (34)$$

which was obtained by adding a field ξ coupled to \hat{O} in the embedding Hamiltonian of Eq. (14) and expressing the variational parameters in terms of the vector \mathbf{x} , see Eq. (26).

To calculate the linear response of the system to the perturbation \hat{O} , we need to evaluate how the saddle-point variational parameters \mathbf{x} of Eq. (33) evolves as a function of ξ . For this purpose, it is convenient to introduce the following functional:

$$\Omega[\xi, \mathbf{x}] = \mathcal{L}_{\text{qp}}[\mathbf{x}] + \mathcal{L}_{\text{mix}}[\mathbf{x}] + \mathcal{L}_{\text{emb}}[\xi, \Phi(\xi, \mathbf{x}), E^c(\xi, \mathbf{x})], \quad (35)$$

where $|\Phi(\xi, \mathbf{x})\rangle$ and $E^c(\xi, \mathbf{x})$ are the ground state of \hat{H}_{emb} and its eigenvalue, respectively, see Eq. (30). Within these definitions, the saddle-point solution of \mathbf{x} for a given ξ , that we call $\mathbf{x}(\xi)$, is defined by:

$$\partial_{\mathbf{x}} \Omega[\xi, \mathbf{x}]|_{(\xi, \mathbf{x}(\xi))} = 0, \quad (36)$$

and the linear response for the operator \hat{O} is given by the following equation (see Appx. D for derivation):

$$\chi_{\mathcal{O}\mathcal{O}} = \chi_{\mathcal{O}\mathcal{O}}^{\text{emb}} + \sum_{\mu} \chi_{\mu\mathcal{O}}^{\text{emb}} \mathcal{M}_{\mu\nu}^{-1} \chi_{\nu\mathcal{O}}^{\text{emb}}, \quad (37)$$

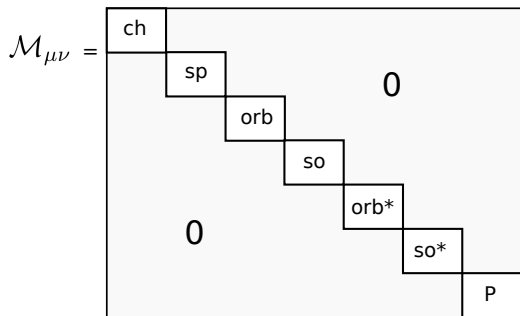


Figure 1. Schematic representation of the block-diagonalized fluctuation matrix in the charge, spin, orbital, spin-orbital, and pairing sector for the three-orbital degenerate Hubbard-Kanamori model (see Eqs. (4)-(5)).

where we introduced the susceptibilities:

$$\chi_{\mathcal{O}\mathcal{O}}^{\text{emb}} = \partial_{\xi} \langle \Phi(\xi, \mathbf{x}) | \hat{\mathcal{O}} | \Phi(\xi, \mathbf{x}) \rangle |_{(\xi=0, \mathbf{x}(\xi=0))}, \quad (38)$$

$$\chi_{\mu\mathcal{O}}^{\text{emb}} = \partial_{x_{\mu}} \langle \Phi(\xi, \mathbf{x}) | \hat{\mathcal{O}} | \Phi(\xi, \mathbf{x}) \rangle |_{(\xi=0, \mathbf{x}(\xi=0))}. \quad (39)$$

The so-called “fluctuation matrix” is:

$$\mathcal{M}_{\mu\nu} = \partial_{x_{\mu}} \partial_{x_{\nu}} \Omega[\xi, \mathbf{x}] |_{(\xi=0, \mathbf{x}(\xi=0))}. \quad (40)$$

Here, the indices μ and ν run through all the variational variables in Eq. (26), i.e., r_s , l_s , d_s , D_s , l_s^c . To keep track of the structure of the fluctuation matrix (where different second order derivatives are computed through different equations, see Appx. E), from now on we will often use these variational variables as matrix subscripts. For example, \mathcal{M}_{D_s, l_s^c} corresponds to the second order derivatives with respect to D_s and l_s^c (see Eq. (E21)).

It is important to note that \mathcal{M} is not invertible. The reason is that the functional Ω is invariant with respect to the gauge transformation (Eq. (H6)), so \mathcal{M} is not unique because of the would-be Goldstone modes. As explained in Appx. I, this redundancy can be systematically resolved by operating a gauge fixing process that removes from the onset of the would-be Goldstone modes [47]. A simpler alternative is to solve the overdetermined linear system (Eq. (40)) by introducing the Moore-Penrose pseudo-inverse of the fluctuation matrix, which we are going to indicate as $\bar{\mathcal{M}}^{-1}$. In terms of the pseudo-inverse, the susceptibility can be formally expressed as follows:

$$\chi_{\mathcal{O}\mathcal{O}} = \chi_{\mathcal{O}\mathcal{O}}^{\text{emb}} + \sum_{\mu\nu} \chi_{\mu\mathcal{O}}^{\text{emb}} \bar{\mathcal{M}}_{\mu\nu}^{-1} \chi_{\nu\mathcal{O}}^{\text{emb}}. \quad (41)$$

Note that Eq. (41) applies for general multiorbital Hubbard models, and the procedure for evaluating each element, Eqs. (38), (39), (40), is described in Appx. E.

We now discuss the application of our formalism to the degenerate three-orbital Hubbard-Kanamori model. For the considered model, the fluctuation matrix \mathcal{M} reduces to a block-diagonal matrix, constructed by seven 5×5 matrices shown schematically in Fig. 1 (one for each

fluctuation channel s), because of the orthonormality of the fluctuation basis $\text{Tr}[\mathbf{h}_s \mathbf{h}_{s'}^{\dagger}] = \delta_{ss'}$. Furthermore, for a given channel s , $\chi_{\mu\mathcal{O}}^{\text{emb}}$ (see Eq. (39)) is nonzero only for the components $\mu = D_s$ and l_s . Therefore, Eq. (41), for a given channel s , can be further simplified to:

$$\chi_{\mathcal{O}_s \mathcal{O}_s} = \chi_{\mathcal{O}_s \mathcal{O}_s}^{\text{emb}} + \chi_{D_s \mathcal{O}_s}^{\text{emb}} \bar{\mathcal{M}}_{D_s D_s}^{-1} \chi_{D_s \mathcal{O}_s}^{\text{emb}} + 2 \chi_{D_s \mathcal{O}_s}^{\text{emb}} \bar{\mathcal{M}}_{D_s l_s^c}^{-1} \chi_{l_s^c \mathcal{O}_s}^{\text{emb}} + \chi_{l_s^c \mathcal{O}_s}^{\text{emb}} \bar{\mathcal{M}}_{l_s^c l_s^c}^{-1} \chi_{l_s^c \mathcal{O}_s}^{\text{emb}}, \quad (42)$$

where $\bar{\mathcal{M}}_{D_s D_s}^{-1}$ denotes the $\mu = D_s$ and $\nu = D_s$ component of $\bar{\mathcal{M}}_{\mu\nu}^{-1}$, and similarly applies to $\bar{\mathcal{M}}_{D_s l_s}^{-1}$ and $\bar{\mathcal{M}}_{l_s^c l_s^c}^{-1}$. We only need to evaluate the 5×5 fluctuation matrix and its pseudo-inversion within each s block to compute the corresponding susceptibility. Note that the block-diagonal structure is not directly applicable to generic systems, because of effects such as orbital differentiation or spin-orbit coupling. In these cases, one has to compute the full fluctuation matrix for calculating response functions.

IV. FERMI-LIQUID APPROXIMATION AND DIAGRAMMATIC APPROACH

The Landau Fermi-liquid theory allows one to describe the thermodynamic properties of metals in terms of an effective non-interacting picture. Importantly, this framework applies only to conserved quantities. In particular, since the superconducting order parameter $\hat{\mathcal{O}}_P$ does not commute with Eq. (1), the corresponding susceptibility is not rigorously expressible in terms of quasiparticle parameters. Nevertheless, as we are going to show below, within the RISB framework, it is possible to derive an approximate (but accurate) expression for the superconducting susceptibility in terms of the quasiparticle Green’s function and interaction vertices. Moreover, the susceptibility can be formulated in terms of the Bethe-Salpeter equation, allowing further diagrammatic analysis for the pairing mechanism.

From the point of view of the RISB methodology, the reason why the superconducting susceptibility cannot be calculated in terms of quasiparticle parameters is that:

$$K_s[\Phi_i, \Delta_i] = \sum_{\alpha\beta} [\mathbf{h}_s]_{\alpha\beta} (\langle \Phi_i | \Xi_{i\alpha}^{\dagger} \Xi_{i\beta} | \Phi_i \rangle - \Delta_{i\alpha\beta}) \neq 0 \quad (43)$$

for $s = P$, i.e., the physical density matrix is, in general, not the same as the quasiparticle density matrix.

Here we propose to modify the spatially inhomogeneous RISB Lagrange function (Eq. (6)) by imposing the constraint:

$$K_s[\Phi_i, \Delta_i] = 0, \quad (44)$$

which is accomplished by introducing additional Lagrange multipliers $\zeta_{i,s}$ into Eq. (26) so the \mathbf{x} vector be-

comes:

$$\begin{aligned} \mathbf{x}_i = & (r_{i,\text{ch}}, l_{i,\text{ch}}, d_{i,\text{ch}}, D_{i,\text{ch}}, l_{i,\text{ch}}^c, \zeta_{i,\text{ch}}, \dots, r_{i,s}, l_{i,s}, \\ & d_{i,s}, D_{i,s}, l_{i,s}^c, \zeta_{i,s}, \dots, r_{i,\text{P}}, l_{i,\text{P}}, d_{i,\text{P}}, D_{i,\text{P}}, l_{i,\text{P}}^c, \zeta_{i,\text{P}}). \end{aligned} \quad (45)$$

We also introduce $\mathbf{x}_{\mathbf{q}}$, which is the momentum conjugate to \mathbf{x}_i .

The Lagrange function now has the following form:

$$\mathcal{L}[\xi, \mathbf{x}, \Phi, E^c] = \mathcal{L}_{\text{qp}}[\xi_{\mathbf{q}}, \mathbf{x}_{\mathbf{q}}] + \mathcal{L}_{\text{mix}}[\mathbf{x}_i] + \mathcal{L}_{\text{emb}}[\mathbf{x}_i, \Phi_i, E_i^c], \quad (46)$$

where

$$\mathcal{L}_{\text{qp}}[\xi_{\mathbf{q}}, \mathbf{x}_{\mathbf{q}}] = -\frac{T}{N} \frac{1}{2} \sum_{\omega_n} \sum_{\mathbf{k}_1 \mathbf{k}_2} \text{Tr} \log \left[-\mathbf{G}_{\omega_n, \mathbf{k}_1, \mathbf{k}_2}^{-1}[\mathbf{x}, \xi] \right], \quad (47)$$

$$\begin{aligned} \mathcal{L}_{\text{emb}}[\mathbf{x}_i, \Phi_i, E_i^c] = & \sum_i \langle \Phi_i(\mathbf{x}_i) | \hat{H}_{\text{emb}}[\mathbf{x}_i] + \frac{1}{2} \sum_{\alpha\beta s} \zeta_{i,s} \mathbf{h}_{s,\alpha\beta} \\ & \hat{\Xi}_{i\alpha}^\dagger \hat{\Xi}_{i\beta} | \Phi_i(\mathbf{x}_i) \rangle + E_i^c (1 - \langle \Phi_i(\mathbf{x}_i) | \Phi_i(\mathbf{x}_i) \rangle), \end{aligned} \quad (48)$$

$$\begin{aligned} \mathcal{L}_{\text{mix}}[\mathbf{x}_i] = & -\sum_i \left[\frac{1}{2} \sum_{ab} (\mathbf{\Lambda}_{iab} + \mathbf{\Lambda}_{iab}^c + \sum_s \zeta_{i,s} \mathbf{h}_{s,ab}) \mathbf{\Delta}_{iab} \right. \\ & \left. + \sum_{a\alpha c} (\mathbf{D}_{ia\alpha} \mathbf{R}_{i\alpha c} [\mathbf{\Delta}(1 - \mathbf{\Delta})]_{ica}^{\frac{1}{2}} + \text{c.c.}) \right], \end{aligned} \quad (49)$$

where we have introduced the physical Green's function:

$$\mathbf{G}_{\omega_n, \mathbf{k}_1, \mathbf{k}_2}[\xi, \mathbf{x}] = \mathbf{R}^\dagger \mathbf{G}_{\omega_n, \mathbf{k}_1, \mathbf{k}_2}^{\text{qp}}[\xi, \mathbf{x}] \mathbf{R} \quad (50)$$

and the quasiparticle Green's function:

$$[\mathbf{G}_{\omega_n, \mathbf{k}_1, \mathbf{k}_2}^{\text{qp}}[\xi, \mathbf{x}]]_{ab}^{-1} = i\omega_n - [H_{\mathbf{k}_1 \mathbf{k}_2}^{\text{qp}}[\mathbf{x}]]_{ab} + \xi_{\mathbf{k}_1 - \mathbf{k}_2} [\mathcal{O}]_{ab}. \quad (51)$$

Similar to the previous section, we also introduced a field $\xi_{\mathbf{k}_1 - \mathbf{k}_2}$ coupled to a generic quasiparticle operator $\hat{\mathcal{O}} = \sum_{ab} \Psi_{\mathbf{k}_1 a}^\dagger [\mathcal{O}]_{ab} \Psi_{\mathbf{k}_2 b}$ into \mathcal{L}_{qp} . This modification will allow us to derive momentum dependent susceptibilities, for investigating the finite momentum (commensurate or incommensurate) instabilities. From now on, we refer to Eq. (44) as the ‘‘quasiparticle constraint.’’

Since utilizing the Lagrange equation Eqs. (47)-(49) amounts to solve the RISB equations Eqs. (27)-(32) within a reduced variational space, the corresponding solution is an approximation to the original one. In principle, enforcing the constraint (Eq. (44)) does not affect the results for the conserving channels, where the fluctuating operator commutes with the Hamiltonian, e.g., the charge and spin channels. However, it reduces slightly the variational freedom when the constraint is imposed on the non-conserving channel, e.g., the pairing channel. Nevertheless, as we are going to show, it is always possible to verify a-posteriori the accuracy of the approximation, by comparison to the formalism without the constraint (see also Appx. J).

It is also interesting to point out that Eq. (44) corresponds to the density matrix mapping constraint in DMET [24]. Therefore, the formalism presented in this section is also applicable to the NIB-DMET, by removing the r_s sector of the fluctuation basis (Eq. (45)) and setting $\mathbf{R} = I$ [25]. This application is discussed in Appx. N.

A. Susceptibility: diagrammatic expression

Here we show how the susceptibility evaluated with the quasiparticle constraint can be expressed in terms of the Feynman diagram in perturbation theory.

Following the procedure in Sec. III C, we introduce the following functional:

$$\begin{aligned} \Omega[\xi, \mathbf{x}] = & \mathcal{L}_{\text{qp}}[\xi_{\mathbf{q}}, \mathbf{x}_{\mathbf{q}}] + \mathcal{L}_{\text{mix}}[\mathbf{x}_i] \\ & + \mathcal{L}_{\text{emb}}[\Phi(\mathbf{x}_i), E^c(\mathbf{x}_i)], \end{aligned} \quad (52)$$

where now \mathcal{L}_{qp} depends on the field $\xi_{\mathbf{q}}$. The linear response for a generic operator is given by the following equation:

$$\begin{aligned} \chi_{\mathcal{O}\mathcal{O}}(\mathbf{q}) = & \frac{T}{2N} \sum_{\mathbf{k}\omega_n} \frac{d}{d\xi_{\mathbf{q}}} \text{Tr} [\mathbf{G}_{\omega_n, \mathbf{k}+\mathbf{q}, \mathbf{k}}[\xi, \mathbf{x}] \bar{\mathcal{O}}] \Big|_{(\xi=0, \mathbf{x}(\xi=0))} \\ = & \chi_{\mathcal{O}\mathcal{O}}^{(0)}(\mathbf{q}) + \sum_{\mu\nu} \chi_{\mu\mathcal{O}}(\mathbf{q}) \mathcal{M}_{\mu\nu}^{-1}(\mathbf{q}) \chi_{\nu\mathcal{O}}(\mathbf{q}), \end{aligned} \quad (53)$$

where the bare susceptibilities are

$$\chi_{\mathcal{O}\mathcal{O}}^{(0)}(\mathbf{q}) = -\frac{T}{2N} \sum_{\mathbf{k}\omega_n} \text{Tr} [\mathbf{G}_{\omega_n, \mathbf{k}+\mathbf{q}} \bar{\mathcal{O}} \mathbf{G}_{\omega_n, \mathbf{k}} \bar{\mathcal{O}}], \quad (54)$$

$$\chi_{\mu\mathcal{O}}(\mathbf{q}) = \frac{T}{2N} \sum_{\mathbf{k}\omega_n} \partial_{x_{\mu, \mathbf{q}}} \text{Tr} [\mathbf{G}_{\omega_n, \mathbf{k}+\mathbf{q}, \mathbf{k}}[\xi, \mathbf{x}] \bar{\mathcal{O}}] \Big|_{(\xi=0, \mathbf{x}(\xi=0))}. \quad (55)$$

Note again that μ runs through all the elements in Eq. (45), and we use the variational parameters as subscripts. We also introduced the saddle-point Green's function $\mathbf{G}_{\omega_n, \mathbf{k}} = \mathbf{R}^\dagger [i\omega_n - H_{\mathbf{k}}^{\text{qp}}]^{-1} \mathbf{R}$ and $\bar{\mathcal{O}} = [\mathbf{R}]^{-1} \mathcal{O} [\mathbf{R}^\dagger]^{-1}$. The fluctuation matrix \mathcal{M} now depends on momentum \mathbf{q} and has an additional component ζ_s (see Eq. (45)). The specific form of \mathcal{M} is given in Appx. E. Furthermore, \mathcal{M} is now an invertible matrix because the quasiparticle constraint breaks the gauge symmetry. Note that Eq. (53) applies for generic multiorbital Hubbard models.

We now discuss the application of our approach to the degenerate three-orbital Hubbard-Kanamori model. As described in the previous section, for the degenerate model considered here, \mathcal{M} is a block-diagonal matrix shown schematically in Fig. 1. Also, from Eqs. (4)-(5) and Eqs. (C7)-(C15), we have $\bar{\mathcal{O}}_s = \bar{\mathbf{h}}_s = [\mathbf{R}]^{-1} \mathbf{h}_s [\mathbf{R}^\dagger]^{-1}$

for each fluctuation channel s . Therefore, the susceptibility can be simplified to:

$$\begin{aligned}\chi_{\mathcal{O}_s \mathcal{O}_s}(\mathbf{q}) &= \chi_{\mathcal{O}_s \mathcal{O}_s}^{(0)}(\mathbf{q}) + \chi_{r_s \mathcal{O}_s}(\mathbf{q}) \mathcal{M}_{r_s r_s}^{-1}(\mathbf{q}) \chi_{r_s \mathcal{O}_s}(\mathbf{q}) \\ &\quad + 2\chi_{r_s \mathcal{O}_s}(\mathbf{q}) \mathcal{M}_{r_s l_s}^{-1}(\mathbf{q}) \chi_{l_s \mathcal{O}_s}(\mathbf{q}) \\ &\quad + \chi_{l_s \mathcal{O}_s}(\mathbf{q}) \mathcal{M}_{l_s l_s}^{-1}(\mathbf{q}) \chi_{l_s \mathcal{O}_s}(\mathbf{q}),\end{aligned}\quad (56)$$

where

$$\begin{aligned}\chi_{r_s \mathcal{O}_s}(\mathbf{q}) &= -\frac{T}{2N} \sum_{\mathbf{k}\omega_n} \text{Tr} [\mathbf{G}_{\omega_n, \mathbf{k}+\mathbf{q}}[\mathbf{R}]^{-1} [(\tilde{\mathbf{h}}_s \epsilon_{\mathbf{k}+\mathbf{q}} \mathbf{R}^\dagger \\ &\quad + \mathbf{R} \epsilon_{\mathbf{k}} \tilde{\mathbf{h}}_s^\dagger) [\mathbf{R}^\dagger]^{-1} \mathbf{G}_{\omega_n, \mathbf{k}} \tilde{\mathbf{h}}_s],\end{aligned}\quad (57)$$

$$\chi_{l_s \mathcal{O}_s}(\mathbf{q}) = -\frac{T}{2N} \sum_{\mathbf{k}\omega_n} \text{Tr} [\mathbf{G}_{\omega_n, \mathbf{k}+\mathbf{q}} \tilde{\mathbf{h}}_s \mathbf{G}_{\omega_n, \mathbf{k}} \tilde{\mathbf{h}}_s] \quad (58)$$

The $\mathcal{M}_{r_s r_s}^{-1}(\mathbf{q})$ denotes the $\mu = r_s$ and $\nu = r_s$ component of $\mathcal{M}_{\mu\nu}^{-1}(\mathbf{q})$ and similarly applies to $\mathcal{M}_{r_s l_s}^{-1}(\mathbf{q})$ and $\mathcal{M}_{l_s l_s}^{-1}(\mathbf{q})$. We only need to evaluate the 6×6 fluctuation matrix and its inversion within each s block to compute the corresponding susceptibility.

To make a connection to perturbation theory, we compare Eq. (56) with the Bethe-Salpeter representation of the susceptibility:

$$\begin{aligned}\chi_{\mathcal{O}_s \mathcal{O}_s}(\mathbf{q}) &= \chi_{\mathcal{O}_s \mathcal{O}_s}^{(0)}(\mathbf{q}) - \left(\frac{-T}{2N}\right)^2 \sum_{\alpha\beta\gamma\delta} \sum_{\mathbf{k}\mathbf{k}'\omega_n\omega_{n'}} [\mathbf{G}_{\omega_n, \mathbf{k}} \tilde{\mathbf{h}}_s \\ &\quad \mathbf{G}_{\omega_n, \mathbf{k}+\mathbf{q}}]_{\beta\alpha} \tilde{\Gamma}_{\alpha\beta\gamma\delta}^s(\mathbf{k}, \mathbf{k}', \mathbf{q}) [\mathbf{G}_{\omega_{n'}, \mathbf{k}'} \tilde{\mathbf{h}}_s \mathbf{G}_{\omega_{n'}, \mathbf{k}'+\mathbf{q}}]_{\delta\gamma}\end{aligned}\quad (59)$$

where $\tilde{\Gamma}_{\alpha\beta\gamma\delta}^s(\mathbf{k}, \mathbf{k}', \mathbf{q})$ is the (reducible) interaction vertex. To extract the $\tilde{\Gamma}_{\alpha\beta\gamma\delta}^s(\mathbf{k}, \mathbf{k}', \mathbf{q})$ from Eq. (56), we introduced the following three-leg vertices:

$$\tilde{\Lambda}_{\alpha\beta r_s}(\mathbf{k}, \mathbf{q}) \equiv \frac{1}{2} [\mathbf{R}]_{\alpha a}^{-1} [\mathbf{R} \tilde{\epsilon}_{\mathbf{k}+\mathbf{q}} \tilde{\mathbf{h}}_s^\dagger + \tilde{\mathbf{h}}_s \tilde{\epsilon}_{\mathbf{k}} \mathbf{R}^\dagger]_{ab} [\mathbf{R}^\dagger]_{b\beta}^{-1}, \quad (60)$$

$$\tilde{\Lambda}_{\alpha\beta l_s} \equiv \frac{1}{2} [\mathbf{R}]_{\alpha a}^{-1} \mathbf{h}_{s, ab} [\mathbf{R}^\dagger]_{b\beta}^{-1}, \quad (61)$$

such that the susceptibilities can be written as:

$$\chi_{r_s \mathcal{O}_s}(\mathbf{q}) = -\frac{T}{N} \sum_{\mathbf{k}\omega_n} \text{Tr} [\mathbf{G}_{\omega_n, \mathbf{k}+\mathbf{q}} \tilde{\Lambda}_{r_s}(\mathbf{k}, \mathbf{q}) \mathbf{G}_{\omega_n, \mathbf{k}} \tilde{\mathbf{h}}_s], \quad (62)$$

$$\chi_{l_s \mathcal{O}_s}(\mathbf{q}) = -\frac{T}{N} \sum_{\mathbf{k}\omega_n} \text{Tr} [\mathbf{G}_{\omega_n, \mathbf{k}+\mathbf{q}} \tilde{\Lambda}_{l_s} \mathbf{G}_{\omega_n, \mathbf{k}} \tilde{\mathbf{h}}_s]. \quad (63)$$

Substituting Eqs. (62) and (63) into Eq. (56), we obtain the interaction vertex (see Eq. (59)):

$$\begin{aligned}\tilde{\Gamma}_{\alpha\beta\gamma\delta}^s(\mathbf{k}, \mathbf{k}', \mathbf{q}) &= -4 (\tilde{\Lambda}_{\alpha\beta r_s}(\mathbf{k}, \mathbf{q}) \tilde{\Lambda}_{\alpha\beta l_s}) \\ &\quad \cdot \begin{pmatrix} \mathcal{M}_{r_s r_s}^{-1}(\mathbf{q}) & \mathcal{M}_{r_s l_s}^{-1}(\mathbf{q}) \\ \mathcal{M}_{r_s l_s}^{-1}(\mathbf{q}) & \mathcal{M}_{l_s l_s}^{-1}(\mathbf{q}) \end{pmatrix} \begin{pmatrix} \tilde{\Lambda}_{\gamma\delta r_s}(\mathbf{k}', \mathbf{q}) \\ \tilde{\Lambda}_{\gamma\delta l_s} \end{pmatrix},\end{aligned}\quad (64)$$

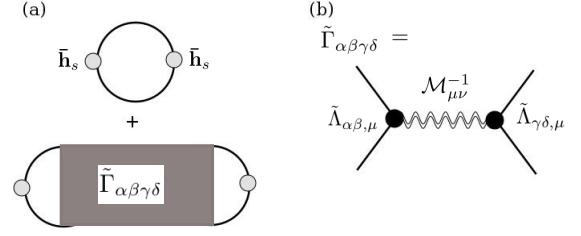


Figure 2. (a) Diagrammatic representation of the susceptibility (Eq. (59)). The thick solid line indicates the Nambu fermionic propagator. The grey circle corresponds to the fluctuation basis $\tilde{\mathbf{h}}_s$, and the grey square corresponds to the quasiparticle interaction vertex $\tilde{\Gamma}_{\alpha\beta\gamma\delta}^s$. (b) Diagrammatic representation of the quasiparticle interaction vertex $\tilde{\Gamma}_{\alpha\beta\gamma\delta}^s$ (Eq. (64)). The double wavy line corresponds to the dressed bosonic propagator containing the infinite summation of the particle-particle or the particle-hole fermionic bubbles. The black circles denote the three-leg vertices $\tilde{\Lambda}_{\alpha\beta\mu}$ (see main text for detail).

describing the effective interaction between quasiparticles mediated by the bosonic propagator $\mathcal{M}_{\mu\nu}^{-1}$ in the corresponding channel.

The diagrammatic representation of Eq. (59) is shown in Fig. 2 (a), where the solid line corresponds to the Nambu propagator, the grey circle corresponds to $\tilde{\mathbf{h}}_s$, and the grey rectangle corresponds to the interaction vertex $\tilde{\Gamma}_{\alpha\beta\gamma\delta}^s(\mathbf{k}, \mathbf{k}', \mathbf{q})$. The diagrammatic representation for the interaction vertex $\tilde{\Gamma}_{\alpha\beta\gamma\delta}^s(\mathbf{k}, \mathbf{k}', \mathbf{q})$ is shown in Fig. 2(b), where the solid circles correspond to the three-leg vertices $\tilde{\Lambda}_{\alpha\beta\mu}$. The double wavy line corresponds to $\mathcal{M}_{\mu\nu}^{-1}(\mathbf{q})$, which can be viewed as the dressed bosonic propagator (see Appx. F) summing the particle-hole bubbles, for $s \in \{\text{ch, sp, orb, so, orb}^*, \text{so}^*\}$, or the particle-particle bubbles, for $s = P$, to the infinite order.

B. Landau Fermi-liquid parameters

We can now calculate the Landau Fermi-liquid parameters for the considered three-orbital degenerate model from Eq. (64). For each channel $s \in \{\text{ch, sp, orb, so, orb}^*, \text{so}^*\}$, we have:

$$\begin{aligned}\Gamma^s(\mathbf{k}, \mathbf{k}', \mathbf{q}) &= -\frac{1}{2Z^2} \left[Z(\epsilon_{\mathbf{k}} + \epsilon_{\mathbf{k}+\mathbf{q}})(\epsilon_{\mathbf{k}'} + \epsilon_{\mathbf{k}'+\mathbf{q}}) \mathcal{M}_{r_s r_s}^{-1}(\mathbf{q}) \right. \\ &\quad + R_0(\epsilon_{\mathbf{k}} + \epsilon_{\mathbf{k}+\mathbf{q}}) \mathcal{M}_{r_s l_s}^{-1}(\mathbf{q}) + R_0(\epsilon_{\mathbf{k}'} + \epsilon_{\mathbf{k}'+\mathbf{q}}) \\ &\quad \left. \mathcal{M}_{r_s l_s}^{-1}(\mathbf{q}) + \mathcal{M}_{l_s l_s}^{-1}(\mathbf{q}) \right],\end{aligned}\quad (65)$$

where we applied $\mathbf{R} = R_0 I$ and $Z = R_0^2$ for the degenerate model considered here. The scattering amplitude for each particle-hole channel s can be evaluated from

$$A_s(\mathbf{q}) = N_F Z^2 \langle \langle \Gamma^s(\mathbf{k}, \mathbf{k}', \mathbf{q}) \rangle \rangle_{\mathbf{k}_F, \mathbf{k}'_F}, \quad (66)$$

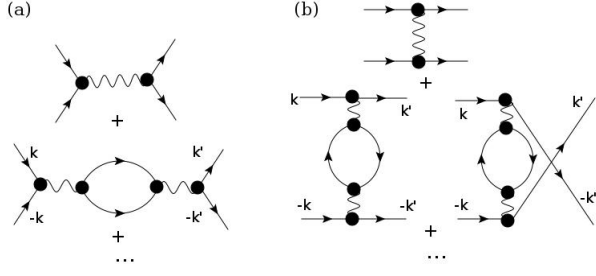


Figure 3. (a) The pairing vertex from the local particle-particle fluctuation (Eq. (70)). (b) The pairing vertex from the particle-hole fluctuations (Eq. (74)). The bubbles are summed to the infinite order. The arrow solid line corresponds to the normal fermionic propagator. The wavy line corresponds to the bare bosonic propagator.

where we introduce the Fermi surface average

$$\langle\langle\Gamma(\mathbf{k}, \mathbf{k}')\rangle\rangle_{\mathbf{k}_F} = \frac{\sum_{\mathbf{k}\mathbf{k}'} \Gamma(\mathbf{k}, \mathbf{k}') \delta_{\mathbf{k}, \mathbf{k}_F} \delta_{\mathbf{k}', \mathbf{k}_F}}{\sum_{\mathbf{k}\mathbf{k}'} \delta_{\mathbf{k}, \mathbf{k}_F} \delta_{\mathbf{k}', \mathbf{k}_F}}. \quad (67)$$

$N_F \equiv \chi_{\mathcal{O}_s \mathcal{O}_s}^{(0)}(0)$ is the density of state at the Fermi-level, which coincides with the bare susceptibility $\chi_{\mathcal{O}_s \mathcal{O}_s}^{(0)}$. The Fermi-liquid parameters F_s can be extracted from the scattering amplitude (see Appx. G)

$$A_s(\mathbf{q}) = \frac{F_s(\mathbf{q})}{1 + F_s(\mathbf{q})}. \quad (68)$$

From the definition of the quasiparticle susceptibility Eq. (59) and Eq. (68), we obtain the random phase approximation (RPA) like expression for the susceptibilities

$$\chi_{\mathcal{O}_s \mathcal{O}_s}(\mathbf{q}) = \frac{\chi_{\mathcal{O}_s \mathcal{O}_s}^{(0)}(\mathbf{q})}{1 + F_s(\mathbf{q})}, \quad (69)$$

for $s \in \{\text{ch, sp, orb, so, orb}^*, \text{so}^*\}$. Note that we have applied the Fermi-surface average over \mathbf{k} and \mathbf{k}' . The divergence of the quasiparticle susceptibilities and the scattering amplitudes can be determined from the condition $F_s(\mathbf{q}) = -1$. Although Eq. (69) has an RPA-like form, the Fermi-liquid parameters are renormalized by the correlation effect for different \mathbf{q} , which provides a more accurate description for strongly correlated systems.

C. Pairing interaction from the particle-particle channel

The reducible pairing vertex in the orbital-antisymmetric spin-triplet pairing channel $s = P$ can be computed by projecting the particle-particle scattering vertex $\tilde{\Gamma}^P$ (Eq. (64)) onto the orbital-antisymmetric

spin-triplet pairing basis \mathbf{h}_P (see Appx. (C2)):

$$\begin{aligned} \Gamma_{\text{pp}}^{\text{sc}}(\mathbf{k}, \mathbf{k}', \mathbf{q} = 0) &= [\mathbf{h}_P^\dagger]_{\alpha\beta} \tilde{\Gamma}_{\alpha\beta\gamma\delta}^P(\mathbf{k}, \mathbf{k}', \mathbf{q} = 0) [\mathbf{h}_P]_{\delta\gamma} \\ &= -\frac{1}{2Z^4} \left[Z(\epsilon_{\mathbf{k}} + \epsilon_{\mathbf{k}})(\epsilon_{\mathbf{k}'} + \epsilon_{\mathbf{k}'}) \mathcal{M}_{r_P r_P}^{-1}(0) \right. \\ &\quad \left. - R_0(\epsilon_{\mathbf{k}} + \epsilon_{\mathbf{k}}) \mathcal{M}_{r_P l_P}^{-1}(0) - R_0(\epsilon_{\mathbf{k}'} + \epsilon_{\mathbf{k}'}) \right. \\ &\quad \left. \mathcal{M}_{r_P l_P}^{-1}(0) + \mathcal{M}_{l_P l_P}^{-1}(0) \right], \quad (70) \end{aligned}$$

where we applied $\mathbf{R} = R_0 I$ and $Z = R_0^2$ for the degenerate model considered here and restrict the pairing at $\mathbf{q} = 0$. The diagrammatic representation for Eq. (70) is shown in Fig. 3(a). In this scattering process, only the particle-particle fermionic bubbles and the local multiplets fluctuation between different particle number sectors in $\mathcal{M}_{\mu\nu}^{-1}$ are involved (the fluctuation basis \mathbf{h}_P and $\tilde{\mathbf{h}}_P$ in Eqs. (E19)-(E26) selects the fluctuation that does not conserve the particle number.)

We can now derive the RPA-like form for the quasiparticle susceptibility. From $\Gamma_{\text{pp}}^{\text{sc}}$, we compute the reducible pairing interaction by averaging the \mathbf{k} and \mathbf{k}' over the Fermi surface

$$\Gamma_{\text{pp}}^{\text{sc}} = Z^2 \langle\langle\Gamma_{\text{pp}}^{\text{sc}}(\mathbf{k}, \mathbf{k}')\rangle\rangle_{\mathbf{k}_F}. \quad (71)$$

The irreducible pairing interaction $\Gamma_{\text{pp}}^{\text{irr}}$ can be extracted from (see Appx. G)

$$\Gamma_{\text{pp}}^{\text{sc}} = \frac{\Gamma_{\text{pp}}^{\text{irr}}}{1 + \Gamma_{\text{pp}}^{\text{irr}} \chi_{\mathcal{O}_P \mathcal{O}_P}^{(0)}}. \quad (72)$$

From the definition of the quasiparticle susceptibility Eq. (59) and Eq. (72), we obtain the RPA-like expression for the pairing susceptibility

$$\chi_P = \frac{\chi_{\mathcal{O}_P \mathcal{O}_P}^{(0)}}{1 + \Gamma_{\text{pp}}^{\text{irr}} \chi_{\mathcal{O}_P \mathcal{O}_P}^{(0)}}. \quad (73)$$

The divergence of the pairing susceptibilities and vertex can be determined from the condition $\Gamma_{\text{pp}}^{\text{irr}} \chi_{\mathcal{O}_P \mathcal{O}_P}^{(0)} = -1$.

D. Pairing interaction from the particle-hole channel

Besides the s -wave pairing induced from the particle-particle vertex, the particle-hole vertices can also induce the local and the non-local pairing through the charge and spin-fluctuation mechanism [63–66]. To compute the irreducible pairing vertex for the orbital-antisymmetric spin-triplet pairing, we again project the particle-hole vertices onto the pairing basis \mathbf{h}_P :

$$\begin{aligned}
\Gamma_{\text{ph}}^{\text{irr}}(\mathbf{k}, \mathbf{k}') &= \sum_{s \in \{\text{ch, sp, orb, so, orb}^*, \text{so}^*\}} [\mathbf{h}_{\text{P}}^\dagger]_{\alpha\gamma} \tilde{\Gamma}_{\alpha\beta\gamma\delta}^s(\mathbf{k}, \mathbf{k}') [\mathbf{h}_{\text{P}}^\dagger]_{\beta\delta} \\
&= \frac{1}{8} \left[\Gamma^{\text{ch}}(\mathbf{k}, \mathbf{k}', \mathbf{q} = \mathbf{k} - \mathbf{k}') + \Gamma^{\text{sp}}(\mathbf{k}, \mathbf{k}', \mathbf{q} = \mathbf{k} - \mathbf{k}') \right. \\
&\quad - \Gamma^{\text{orb}}(\mathbf{k}, \mathbf{k}', \mathbf{q} = \mathbf{k} - \mathbf{k}') - \Gamma^{\text{so}}(\mathbf{k}, \mathbf{k}', \mathbf{q} = \mathbf{k} - \mathbf{k}') \\
&\quad - \frac{5}{3} \Gamma^{\text{orb}^*}(\mathbf{k}, \mathbf{k}', \mathbf{q} = \mathbf{k} - \mathbf{k}') - \frac{5}{3} \Gamma^{\text{so}^*}(\mathbf{k}, \mathbf{k}', \mathbf{q} = \mathbf{k} - \mathbf{k}') \\
&\quad \left. + (\mathbf{k}' \rightarrow -\mathbf{k}') \right], \tag{74}
\end{aligned}$$

where the charge, spin, orbital, and spin-orbital scattering vertices $\tilde{\Gamma}^s$ are defined in Eq. (65). The diagrammatic representation for Eq. (74) is shown in Fig. 3(b), where the $\mathcal{M}_{r_s t_s}^{-1}$, $\mathcal{M}_{r_s l_s}^{-1}$, and $\mathcal{M}_{l_s l_s}^{-1}$ contain the summation of the particle-hole bubbles to the infinite order (see Appx. F), and we include both the direct and the exchange (crossing) diagrams. The irreducible pairing interaction from the particle-hole channel can be computed from:

$$\Gamma_{\text{ph}}^{\text{irr}} = Z^2 \langle \langle \Gamma_{\text{ph}}^{\text{irr}}(\mathbf{k}, \mathbf{k}') \rangle \rangle_{\mathbf{k}_F}, \tag{75}$$

where we assume an s -wave pairing to compare with the local pairing fluctuation mechanism in the previous section.

V. RESULTS AND DISCUSSION

A. Superconducting phase diagram

In this subsection, we apply our RISB saddle-point approximation and fluctuation approach to the degenerate three-orbital Hubbard-Kanamori model with Hund's coupling $J = U/4$, which serves as an effective model for Hund's metals. We will focus on the order parameter $\langle \hat{\mathcal{O}}_{\text{P}} \rangle$ computed from Eq. (19) and the pairing susceptibility χ_{P} computed from Eq. (42).

Figure 4 (a) shows the intensity plot of the spin-triplet pairing order parameter $\langle \hat{\mathcal{O}}_{\text{P}} \rangle$ at $T = 0.0005t$. The peak of the order parameters locates at the so-called Hund's metal crossover, where the quasiparticle weights Z decrease significantly, as shown in Fig. 4 (c) and (d) for selected fillings $n = 1.6, 2.0, 2.4$, and 2.8 . The faster the decrease in Z , the stronger the enhancement in the pairing order parameters $\langle \hat{\mathcal{O}}_{\text{P}} \rangle$. The normal state in the superconducting regime can be viewed as Hund's metals, where the quasiparticle weight is small, and the local multiplet is populated with high spin states, favoring the local spin-triplet pairing [16, 53, 67–69].

We also show the uniform pairing susceptibility χ_{P} evaluated from the fluctuation technique in Fig. 4 (b). The pairing susceptibility is initially positive at small Coulomb interaction U and diverges at the critical point.

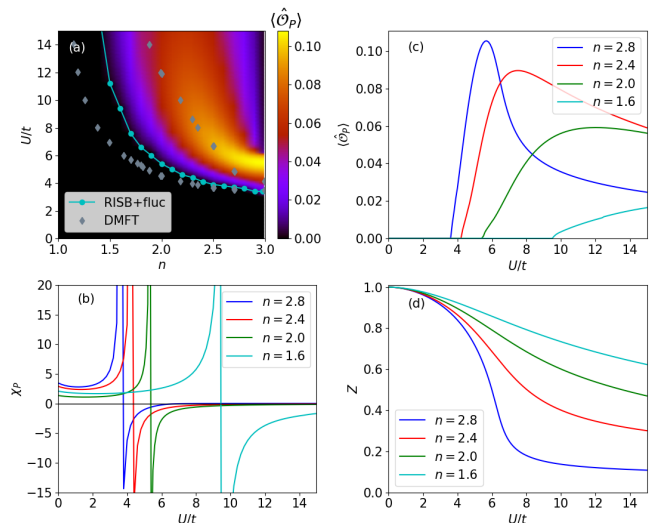


Figure 4. (a) The density plot of the s -wave spin-triplet superconducting order parameter $\langle \hat{\mathcal{O}}_{\text{P}} \rangle$ as a function of electron filling n and Coulomb interaction U with $J = U/4$ at $T = 0.0005t$. The cyan line is the phase boundary determined from the instability in the pairing susceptibility χ_{P} . (b) The uniform pairing susceptibility χ_{P} for $n = 2.8, 2.4, 2.0, 1.6$. (c) The spin-triplet superconducting order parameters $\langle \hat{\mathcal{O}}_{\text{P}} \rangle$ for $n = 2.8, 2.4, 2.0, 1.6$. (d) The quasiparticle weight Z for $n = 2.8, 2.4, 2.0, 1.6$.

Then, the pairing susceptibility turns negative, indicating the instability towards the s -wave spin-triplet ordering state. The phase boundary determined from the divergence of the pairing susceptibility is shown in Fig. 4 (a), which agrees with the onset of the mean-field order parameters indicating the consistency of our approach. We also compare our phase diagram with the DMFT results on a Bethe lattice at $T = 0.04t$ rescaled to the 2D bandwidth $W = 8t$ in Fig. 4 (a). While the RISB superconducting regime is broader than the DMFT results, the overall phase diagram agrees qualitatively with the DMFT [53].

We now turn to the finite-temperature phase diagram for the s -wave spin-triplet pairing state. Figure 5 (a) shows the intensity plot of the s -wave spin-triplet order parameters $\langle \hat{\mathcal{O}}_{\text{P}} \rangle$ at $U = 8t$ as a function of electron filling n and temperature T . The superconducting region has a dome shape structure, where the maximum T_c locates around $n = 2.5$. Figure 5 (b) shows the uniform pairing susceptibility χ_{P} computed from the fluctuation approach for filling $n = 2.0, 2.4$, and 2.8 as a function of temperature T . With decreasing T , the pairing susceptibility increases and diverges at the critical temperature T_c . The critical temperature obtained from the divergence of the pairing susceptibility agrees with the onset of the mean-field order parameters, as shown in Fig. 5 (a). We also compare our phase diagram with the DMFT results on a Bethe lattice in Fig. 5 (a) corresponding to $U = 6t$ rescaled to the 2D bandwidth $W = 8t$ consid-

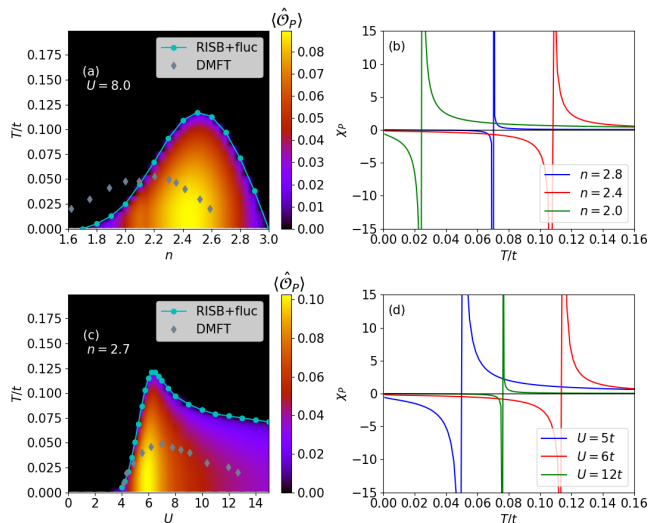


Figure 5. (a) The density plot of the s -wave spin-triplet superconducting order parameter $\langle \hat{O}_P \rangle$ as a function of electron filling n and temperature T at $U = 8$ and $J = U/4$. The cyan line is the phase boundary determined from the instability of the pairing susceptibility χ_P . (b) The uniform pairing susceptibility χ_P for $n = 2.8, 2.4, 2.0$. (c) The density plot of the spin-triplet superconducting order parameter $\langle \hat{O}_P \rangle$ as a function of Coulomb interaction U and temperature T with $n = 2.7$ and $J = U/4$. The cyan line is the phase boundary determined from the instability of the pairing susceptibility χ_P . (d) The uniform pairing susceptibility χ_P for $U = 5t, 6t, 12t$.

ered here. [53]. Both methods generate a dome shape structure where the peak in RISB is closer to half-filling.

Figure 5 (c) shows the intensity plot of the s -wave spin-triplet pairing order parameters $\langle \hat{O}_P \rangle$ as a function of Coulomb interaction U and $J = U/4$ at filling $n = 2.7$. The critical temperature T_c peaks around $U = 6t$, which is around the Hund's metal crossover. Figure 5 (d) shows the corresponding uniform pairing susceptibility computed from the fluctuation approach for $U = 5t, 6t, 12t$. The pairing susceptibility diverges at T_c and turns negative, indicating the instability towards the s -wave spin-triplet pairing states. The T_c obtained from the divergence of the susceptibility again agrees with the onset of the mean-field order parameters, as shown in Fig. 5 (c). We also compare our phase diagram with the DMFT results on a Bethe lattice in Figure 5 (c) at $n = 2.0$ to match with our critical U_c at $T = 0.0005t$. The phase diagrams obtained from both methods are again similar with a dome shape structure where the T_c peaks around the Hund's crossover.

Note that there are two main reasons for expecting qualitative agreement (but quantitative agreement) between our RISB results and the DMFT results of Ref. [53]. The first reason is that RISB (equivalently GA) is essentially a variational approximation to DMFT, in the sense that it is variational in the limit of infinite dimension [70], where DMFT is exact. Also, RISB can be

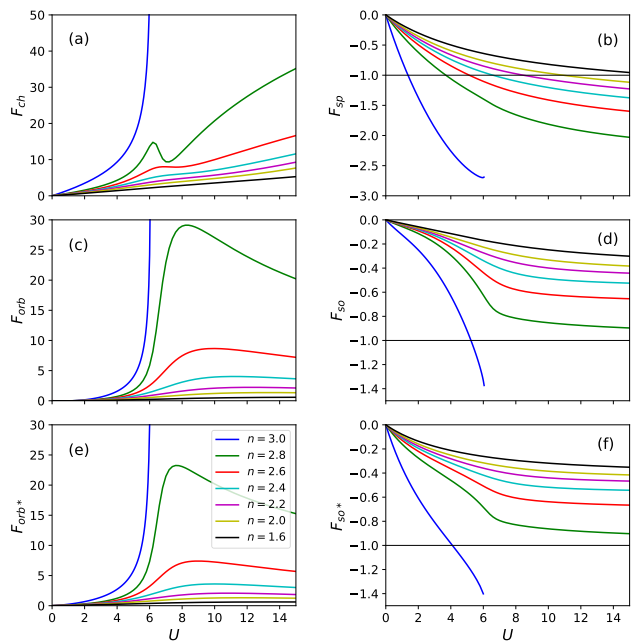


Figure 6. The Landau parameters in the (a) charge, (b) spin, (c) orbital, (d) spin-orbital, (e) orbital*, and (f) spin-orbital* channel defined in Eq. (5) as a function of coulomb interaction U and $J = U/4$ for filling $n = 3.0, 2.8, 2.6, 2.4, 2.2, 2.0, 1.6$ and $T = 0.0005t$.

viewed as an approximation to DMFT, from a quantum embedding perspective, where the uncorrelated bath has the same number of orbitals as the impurity (while the bath is infinite in DMFT). Hence, RISB is expected to be less accurate (but more efficient) compared to DMFT. Nevertheless, we note that, in this work, we assumed a 2D square lattice, while a Bethe lattice was used in Ref. [53]. In fact, it is known that different lattice structures can lead to quantitative differences in the results, but the qualitative behaviors are generally similar [71].

B. Landau parameter and pairing interaction

For studying the pairing mechanism, it is instructive to investigate the quasiparticle interaction vertex in the spin, charge, orbital, spin-orbital, and pairing channel. To obtain these quantities, we applied the Fermi-liquid approximation in Sec. IV, which reproduces the exact physical susceptibility, as shown in Appx. J.

Let us first discuss the charge, spin, orbital, and spin-orbital fluctuation, encoded in the Landau parameters F_s . The Landau parameters F_s in each channel are shown in Fig. 6. We found that the Landau parameters in the charge F_{ch} and orbital F_{orb} (orb*) channels show a peak around the Hund's crossover and diverges at the Mott transition at $n = 3$. The kink in F_{ch} corresponds to the possible phase separation instability found in the previous slave-spin study [72]. Moreover, we found the

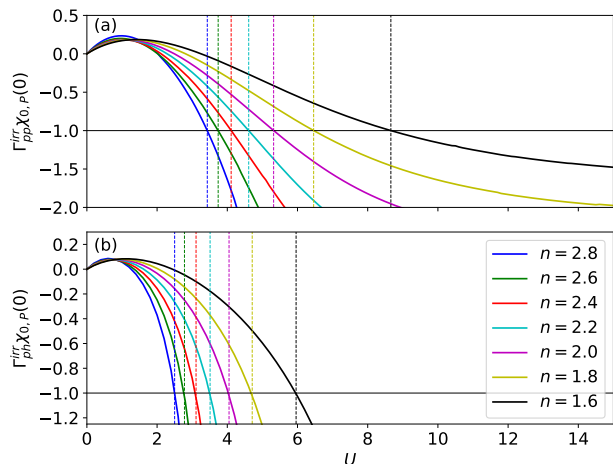


Figure 7. (a) The irreducible particle-particle s -wave spin-triplet pairing vertex $\Gamma_{pp}^{\text{irr}}\chi_{O_P}^{(0)}$ as a function of Coulomb interaction U and $J = U/4$ for filling $n = 2.8, 2.6, 2.4, 2.2, 2.0, 1.8, 1.6$ and temperature $T = 0.0005t$. (b) The irreducible particle-hole s -wave spin-triplet pairing vertex $\Gamma_{ph}^{\text{irr}}\chi_{O_P}^{(0)}$ with the same parameters setting. The vertical dashed lines indicate the critical U_c determined from $\Gamma_{pp}^{\text{irr}}\chi_{O_P}^P = -1$, signaling the divergence of the superconducting susceptibility and the scattering amplitude.

instability towards the ferromagnetic ordering $F_{\text{sp}} = -1$ for a wide range of electron filling. Consequently, F_{sp} is the dominant fluctuation in the particle-hole channel. In addition, the spin-orbital channel $F_{\text{so}(\text{so}^*)}$ also shows a subleading instability at $n = 3$.

We now turn to the irreducible pairing vertex in the particle-particle channel Γ_{pp}^{irr} originated purely from the local pairing fluctuation describing the superconducting instability. Figure 7 (a) shows the behavior of the pairing interaction Γ_{pp}^{irr} in the particle-particle channel as a function of Coulomb interaction U . The condition $\Gamma_{pp}^{\text{irr}}\chi_{O_P}^{(0)} = -1$ indicates the divergence in the pairing susceptibility. In the weak-coupling limit, i.e., $U \ll t$, Γ_{pp}^{irr} follows the bare pairing interaction $U - 3J$ for all the electron filling n . With increasing U , the effective interactions for different electronic filling are renormalized to smaller values and eventually become negative signaling the instability towards the pairing states. The pairing instability determined from Γ_{pp}^{irr} locates around the Hund's metal crossover as discussed in the previous subsection. On the other hand, as shown in Fig. 7 (b), the pairing instability determined from the particle-hole scattering channel Γ_{ph}^{irr} takes place at a much lower U below the Hund's metal crossover. Consequently, the particle-hole spin-fluctuation mechanism cannot explain the pairing instability around Hund's metal crossover. The strong attraction in Γ_{ph}^{irr} is, however, related to the ferromagnetic instability, as shown in Fig. 6(b).

VI. CONCLUSIONS

On the basis of the fluctuation approach around the RISB normal state saddle-point, we developed an efficient method to compute general susceptibilities, quasi-particle interaction vertex, Fermi-liquid parameters, and pairing interaction for the multiorbital Hubbard model. The method has an RPA-like efficiency and a similar accuracy compared to DMFT for correlated systems.

We applied our method to the degenerate three-orbital Hubbard-Kanamori model to investigate the origin of the s -wave orbital-antisymmetric spin-triplet pairing in Hund's metal, previously found in the DMFT studies [53]. We showed that, in agreement with DMFT, the pairing susceptibility of the s -wave spin-triplet pairing states diverges around the Hund's metal crossover. The phase diagram is in good qualitative agreement with DMFT. By computing the pairing interaction considering the particle-particle and the particle-hole scattering channel, we identified that the origin of the superconducting pairing around Hund's crossover arises from the particle-particle channel, containing the local electron pair fluctuation between different particle-number sectors of the local Hilbert space. The pairing interaction is strongly renormalized in the incoherent Hund's metal regime and becomes negative. On the other hand, the particle-hole spin-fluctuation mechanism induces an s -wave pairing instability already for a smaller value of Coulomb interaction, before entering the Hund's regime.

The local interorbital pairing mechanisms revealed in this work can be applied to the s -wave orbital-antisymmetric spin-triplet pairing states proposed for Sr_2RuO_4 [59, 60, 73–75] and KFe_2As_2 [76, 77], where the interplay between the Hund's rule coupling and the spin-orbital coupling leads to intriguing gap structures on the Fermi surface. Our approach provides an efficient route for investigating the pairing mechanism for these materials, with the combination of density functional theory. The general formalism that we presented is also applicable for different purposes. For example, it could be utilized for investigating the response functions in the correlation-induced topological materials, e.g., the topological Kondo and topological Mott insulators [22, 78–80], and the recently proposed topological iron-based superconductors [81, 82]. In addition, the diagrammatic approach proposed in this work may serve as a basis for the non-local extensions beyond RISB, similarly to the diagrammatic approaches beyond DMFT [83]. Finally, our formalism can be applied to the NIB-DMET and other similar quantum embedding methods [84–86].

ACKNOWLEDGMENTS

This work was supported by the Computational Materials Sciences Program funded by the US Department of Energy, Office of Science, Basic Energy Sciences, Materials Sciences and Engineering division. N.L. gratefully

acknowledges support from the Novo Nordisk Foundation through the Exploratory Inter-disciplinary Synergy Programme project NNF19OC0057790, and from the VILLUM FONDEN through the Villum Experiment project 00028019 and the Centre of Excellence for Dirac Materials (Grant. No. 11744).

Appendix A: Gell-Mann matrices

We use the following convention for the Gell-Mann matrices

$$\begin{aligned} \lambda^1 &= \begin{pmatrix} 0 & 1 & 0 \\ 1 & 0 & 0 \\ 0 & 0 & 0 \end{pmatrix}, \lambda^4 = \begin{pmatrix} 0 & -i & 0 \\ i & 0 & 0 \\ 0 & 0 & 0 \end{pmatrix}, \lambda^7 = \begin{pmatrix} 1 & 0 & 0 \\ 0 & -1 & 0 \\ 0 & 0 & 0 \end{pmatrix}, \\ \lambda^2 &= \begin{pmatrix} 0 & 0 & 1 \\ 0 & 0 & 0 \\ 1 & 0 & 0 \end{pmatrix}, \lambda^5 = \begin{pmatrix} 0 & 0 & -i \\ 0 & 0 & 0 \\ i & 0 & 0 \end{pmatrix}, \lambda^8 = \frac{1}{\sqrt{3}} \begin{pmatrix} 1 & 0 & 0 \\ 0 & 1 & 0 \\ 0 & 0 & -2 \end{pmatrix}, \\ \lambda^3 &= \begin{pmatrix} 0 & 0 & 0 \\ 0 & 0 & 1 \\ 0 & 1 & 0 \end{pmatrix}, \lambda^6 = \begin{pmatrix} 0 & 0 & 0 \\ 0 & 0 & -i \\ 0 & i & 0 \end{pmatrix}, \lambda^0 = \begin{pmatrix} 1 & 0 & 0 \\ 0 & 1 & 0 \\ 0 & 0 & 1 \end{pmatrix}, \end{aligned} \quad (\text{A1})$$

where $\lambda^1, \lambda^2, \lambda^3$ describe the symmetric interorbital interactions or pairings; $\lambda^4, \lambda^5, \lambda^6$ describe the anti-symmetric interorbital interactions or pairings; $\lambda^7, \lambda^8, \lambda^0$ describe the intraorbital interactions or pairings. This set of matrices is the most general basis that parameterizes the 3×3 quadratic operators in the orbital space for three-orbital models. In the degenerate three-orbital Hubbard-Kanamori model, the $O(3)$ symmetry implies that the order parameters corresponds to the symmetric interorbital fluctuations λ_1, λ_2 , and λ_3 are identical to each other. Similarly, the order parameters corresponds to the antisymmetric interorbital fluctuations λ_4, λ_5 , and λ_6 are identical to each other.

Appendix B: Rotationally-invariant slave-boson Nambu formalism

In this section, we outline the basis of the RISB Nambu formalism. We start from a generic multiorbital Hubbard model in the Nambu notation:

$$\hat{H} = \frac{1}{2} \sum_{\mathbf{k}} \Xi_{\mathbf{k}\alpha}^\dagger \tilde{\epsilon}_{\mathbf{k},\alpha\beta} \Xi_{\mathbf{k}\beta} + \sum_i \hat{H}_{\text{loc}}[\{d_{i\alpha\sigma}^\dagger, d_{i\alpha\sigma}\}], \quad (\text{B1})$$

where

$$\tilde{\epsilon}_{\mathbf{k},\alpha\beta} = \begin{pmatrix} \epsilon_{\mathbf{k}} & 0 \\ 0 & -\epsilon_{-\mathbf{k}}^* \end{pmatrix} \quad (\text{B2})$$

is the energy dispersion in the Nambu basis. We also define the Nambu spinor $\Xi_{\mathbf{k}}^\dagger = (d_{\mathbf{k}1\uparrow}^\dagger, d_{\mathbf{k}1\downarrow}^\dagger, \dots, d_{\mathbf{k}M\uparrow}^\dagger, d_{\mathbf{k}M\downarrow}^\dagger, d_{-\mathbf{k}1\uparrow}, d_{-\mathbf{k}1\downarrow}, \dots, d_{-\mathbf{k}M\uparrow}, d_{-\mathbf{k}M\downarrow})$, where M is the total number of orbitals. The H_{loc} contains the generic local one-body and two-body interactions.

Within RISB framework, the physical operators $\Xi_{i\alpha}$ is mapped to the product of a renormalization matrix and a quasiparticle Nambu spinor:

$$\Xi_{i\alpha}^\dagger = \sum_a \mathbf{R}_{ia\alpha} [\Phi_i^\dagger, \Phi_i] \Psi_{ia}^\dagger, \quad (\text{B3})$$

where the quasiparticle spinor is $\Psi_i^\dagger = (f_{i1\uparrow}^\dagger, f_{i1\downarrow}^\dagger, \dots, f_{iM\uparrow}^\dagger, f_{iM\downarrow}^\dagger, f_{i1\uparrow}, f_{i1\downarrow}, \dots, f_{iM\uparrow}, f_{iM\downarrow})$, and the renormalization matrix has the following form [62, 87, 88]:

$$\mathbf{R}_{ia\alpha} [\Phi_i^\dagger, \Phi_i] = \sum_b \text{Tr}[\Phi_i^\dagger \Xi_{i\alpha} \Phi_i \Psi_{ib}^\dagger] [\Delta_i (1 - \Delta_i)]_{ba}^{-\frac{1}{2}}, \quad (\text{B4})$$

where

$$[\Delta_i]_{ab} = \text{Tr}[\Phi_i^\dagger \Phi_i \Psi_{ia}^\dagger \Psi_{ib}] \quad (\text{B5})$$

corresponds to the local quasiparticle Nambu density matrix, and $[\Phi_i]_{An}$ is the slave-boson amplitude matrix.

We also define the matrices $[\Xi_{i\alpha}]_{AB} = \langle A | \hat{\Xi}_{i\alpha} | B \rangle$ and $[\Psi_{i\alpha}]_{nm} = \langle n | \hat{\Psi}_{i\alpha} | m \rangle$ for the fermionic operator in the arbitrary local many-body basis $|A\rangle$ and the local Fock basis $|n\rangle$, respectively [9, 21]. The local interactions can be expressed in terms of the bosonic amplitudes as [9]

$$\hat{H}_{\text{loc}} = \sum_{ABn} [\Phi]_{Bn} [\Phi]_{nA}^\dagger [H_{\text{loc}}]_{AB}, \quad (\text{B6})$$

where $[H_{\text{loc}}]_{AB} = \langle A | \hat{H}_{\text{loc}} | B \rangle$.

In order to select the physical states out of the enlarged boson and quasiparticle Hilbert space, one has to enforce the following RISB constraints [9, 62]

$$\text{Tr}[\Phi_i \Phi_i^\dagger] = 1, \quad (\text{B7})$$

$$[\Delta_i]_{ab} = \langle \hat{\Psi}_{ia}^\dagger \hat{\Psi}_{ib} \rangle = \text{Tr}[\Phi_i^\dagger \Phi_i \Psi_{ia}^\dagger \Psi_{ib}]. \quad (\text{B8})$$

The first constraint limits the Hilbert space to the single-boson states, while the second constraint ensures the rotational invariance of the quasiparticle density matrix under the gauge transformation (see Appx. H).

With the RISB representations and constraints (Eqs (B3)-(B8)), the RISB Lagrangian for the generic Hubbard model (Eq. (B1)) can be expressed as:

$$\begin{aligned}
\mathcal{L}[\Phi, \mathbf{R}, \mathbf{\Lambda}; \mathbf{D}, \mathbf{\Lambda}^c, E^c, \Delta] &= \frac{-T}{N} \frac{1}{2} \sum_{\mathbf{k}_1 \mathbf{k}_2 \omega_n} \text{Tr} \log \left[-i\omega_n + H_{\mathbf{k}_1 \mathbf{k}_2}^{\text{qp}} \right] e^{i\omega_n 0^+} + \sum_i \text{Tr} \left[\Phi_i \Phi_i^\dagger H_{\text{loc}} \right. \\
&+ \left. \left(\sum_{a\alpha} [\mathbf{D}_i]_{a\alpha} \Phi_i^\dagger \Xi_{i\alpha}^\dagger \Phi_i \Psi_{ia} + \text{H.c.} \right) + \sum_{ab} \frac{1}{2} [\mathbf{\Lambda}_i^c]_{ab} \Phi_i^\dagger \Phi_i \Psi_{ia}^\dagger \Psi_{ib} \right] + E_i^c \left(\text{Tr} \left[\Phi_i \Phi_i^\dagger \right] - 1 \right) \\
&- \sum_i \left[\sum_{ab} \frac{1}{2} \left([\mathbf{\Lambda}_i]_{ab} + [\mathbf{\Lambda}_i^c]_{ab} \right) [\mathbf{\Delta}_i]_{ab} + \sum_{c\alpha} \left([\mathbf{D}_i]_{a\alpha} [\mathbf{R}_i]_{c\alpha} [\mathbf{\Delta}_i (1 - \mathbf{\Delta}_i)]_{ca}^{1/2} + \text{c.c.} \right) \right], \quad (\text{B9})
\end{aligned}$$

where the original kinetic hopping term in Eq. (B1) is described by the quasiparticle Hamiltonian:

$$[H_{\mathbf{k}_1 \mathbf{k}_2}^{\text{qp}}]_{ab} = \frac{1}{N} \sum_{\mathbf{k}} [\mathbf{R}_{\mathbf{k}_1 - \mathbf{k}} \tilde{\epsilon}_{\mathbf{k}} \mathbf{R}_{\mathbf{k}_2 - \mathbf{k}}^\dagger]_{ab} + [\mathbf{\Lambda}_{\mathbf{k}_1 - \mathbf{k}_2}]_{ab}, \quad (\text{B10})$$

while the local interaction \hat{H}_{loc} in Eq. (B1) is mapped to the slave-boson representation $\text{Tr}[\Phi_i \Phi_i^\dagger H_{\text{loc}}]$. The $\mathbf{\Lambda}_i$, $\mathbf{\Lambda}_i^c$, \mathbf{D}_i , E_i^c are the Lagrange multipliers enforcing the RISB constraints (Eqs. (B7) and (B8)) and the structure of the \mathbf{R}_i matrix (Eq. (B4)). Note that all these single-particle matrices contains the particle, hole, and anomalous sector defined as follows:

$$\mathbf{R}_i = \begin{bmatrix} R_i & Q_i^* \\ Q_i & R_i^* \end{bmatrix}, \quad (\text{B11})$$

$$\mathbf{\Lambda}_i = \begin{bmatrix} \Lambda_i & \Lambda_i' \\ \Lambda_i'^\dagger & -\Lambda_i^* \end{bmatrix}, \quad (\text{B12})$$

$$\mathbf{\Lambda}_i^c = \begin{bmatrix} \Lambda_i^c & \Lambda_i^{c'} \\ \Lambda_i^{c'\dagger} & -\Lambda_i^{c*} \end{bmatrix}, \quad (\text{B13})$$

$$\mathbf{D}_i = \begin{bmatrix} D_i & D_i'^* \\ D_i' & D_i^* \end{bmatrix}, \quad (\text{B14})$$

$$\mathbf{\Delta}_i = \begin{bmatrix} \Delta_i & \Delta_i' \\ \Delta_i'^\dagger & (\mathbf{1} - \Delta_i) \end{bmatrix}. \quad (\text{B15})$$

The $\mathbf{\Lambda}_i$, $\mathbf{\Lambda}_i^c$ and $\mathbf{\Delta}_i$ are Hermitian matrices, and the \mathbf{R}_i and \mathbf{D}_i are non-Hermitian matrices. These single-particle matrices are parameterized by Eqs. (21)-(25) utilizing the matrix basis \mathbf{h}_s and $\tilde{\mathbf{h}}_s$, whose structure (for the three-orbital degenerate Hubbard-Kanamori model) is discussed in Sec. C 2.

The slave-boson amplitude can be constructed from the symmetry adaptive basis ϕ_{ip} :

$$[\Phi_i]_{An} = \sum_p c_p [\phi_{ip}]_{An} \quad (\text{B16})$$

where

$$\text{Tr}[\phi_{ip}^\dagger \phi_{ip'}] = \delta_{p,p'} \quad p, p' = 1, \dots, N_\phi, \quad (\text{B17})$$

and the matrix basis commutes with all the symmetry operation in the group G of the given problem, i.e., $[\phi_{ip}, R(g)] = 0 \quad \forall g \in G$. The procedure for determining ϕ_{ip} is discussed in Appx. C 1.

1. Embedding mapping

We now introduce the embedding wavefunction [21]

$$|\Phi_i\rangle = \sum_{An} e^{i(\pi/2)N_n(N_n-1)} [\Phi_i]_{An} U_{\text{PH}} |A\rangle |n\rangle, \quad (\text{B18})$$

where U_{PH} is the particle-hole transformation on the bath site and N_n is the particle number of Fock state $|n\rangle$. Substituting the following identities to Eq. (B9):

$$\text{Tr}[\Phi_i \Phi_i^\dagger H_{\text{loc}}] = \langle \Phi_i | \hat{H}_{\text{loc}} [\hat{d}_{i\alpha}^\dagger, \hat{d}_{i\alpha}] | \Phi_i \rangle \quad (\text{B19})$$

$$\text{Tr}[\Phi_i^\dagger \Xi_{i\alpha}^\dagger \Phi_i \Psi_{ia}] = \sum_b \langle \Phi_i | \hat{\Xi}_{i\alpha}^\dagger \hat{\Psi}_{ib} | \Phi_i \rangle \bar{I}_{ba} \quad (\text{B20})$$

$$\text{Tr}[\Phi_i^\dagger \Phi_i \Psi_{ia}^\dagger \Psi_{ib}] = \sum_{cd} \bar{I}_{bc} \langle \Phi_i | \hat{\Psi}_{ic} \hat{\Psi}_{id}^\dagger | \Phi_i \rangle \bar{I}_{da}, \quad (\text{B21})$$

where

$$\bar{I} = \begin{pmatrix} \mathbf{1} & 0 \\ 0 & -\mathbf{1} \end{pmatrix}, \quad (\text{B22})$$

and $\mathbf{1}$ is the identity matrix, we obtained the RISB Lagrangian in terms of $|\Phi_i\rangle$ in Eq. (6) in the main text.

Appendix C: Variational basis

In this section, we describe the construction of our variational many-body basis ϕ_p and the single-particle basis \mathbf{h}_s and $\tilde{\mathbf{h}}_s$ of our fluctuation approach to the degenerate three-orbital Hubbard-Kanamori model.

1. Many-body basis

For the charge, spin, orbital, and spin-orbital fluctuations, we construct the many-body basis in Eq. (B16)

(N, L, S)	Degeneracy	E_Γ	$\Phi_{\Gamma n}$
$(0, 0, 0)$	1	0	$\Phi(E_{000})$ $\Phi(E_{000}; 2)$ $\Phi(E_{000}; 4)$
$(1, 1, \frac{1}{2})$	6	0	$\Phi(E_{11\frac{1}{2}})$ $\Phi(E_{11\frac{1}{2}}; 2)$ $\Phi(E_{11\frac{1}{2}}; 4)$
$(2, 2, 0)$	5	$U - J$	$\Phi(E_{220})$ $\Phi(E_{220}; -2)$ $\Phi(E_{220}; 2)$ $\Phi(E_{220}; 4)$
$(2, 1, 1)$	9	$U - 3J$	$\Phi(E_{211})$ $\Phi(E_{211}; -2)$ $\Phi(E_{211}; 2)$
$(2, 0, 0)$	1	$U + 2J$	$\Phi(E_{200})$ $\Phi(E_{200}; 2)$ $\Phi(E_{200}; 4)$
$(3, 2, \frac{1}{2})$	10	$3U - 6J$	$\Phi(E_{32\frac{1}{2}})$ $\Phi(E_{32\frac{1}{2}}; -2)$ $\Phi(E_{32\frac{1}{2}}; 2)$
$(3, 1, \frac{1}{2})$	6	$3U - 4J$	$\Phi(E_{31\frac{1}{2}})$ $\Phi(E_{31\frac{1}{2}}; -2)$ $\Phi(E_{31\frac{1}{2}}; 2)$
$(3, 0, \frac{3}{2})$	4	$3U - 9J$	$\Phi(E_{30\frac{3}{2}})$ $\Phi(E_{30\frac{3}{2}}; -2)$ $\Phi(E_{30\frac{3}{2}}; 2)$
$(4, 2, 0)$	5	$6U - 11J$	$\Phi(E_{420})$ $\Phi(E_{420}; -4)$ $\Phi(E_{420}; -2)$ $\Phi(E_{420}; 2)$
$(4, 1, 1)$	9	$6U - 13J$	$\Phi(E_{411})$ $\Phi(E_{411}; -4)$ $\Phi(E_{411}; -2)$ $\Phi(E_{411}; 2)$
$(4, 0, 0)$	1	$U + 2J$	$\Phi(E_{400})$ $\Phi(E_{400}; -4)$ $\Phi(E_{400}; -2)$ $\Phi(E_{400}; 2)$
$(5, 1, \frac{1}{2})$	6	$10U - 20J$	$\Phi(E_{51\frac{1}{2}})$ $\Phi(E_{51\frac{1}{2}}; -4)$ $\Phi(E_{51\frac{1}{2}}; -2)$
$(6, 0, 0)$	1	$15U - 30J$	$\Phi(E_{600})$ $\Phi(E_{600}; -4)$ $\Phi(E_{600}; -2)$

Table I. Quantum numbers (N, L, S) , degeneracy, Eigenvalues, and the corresponding slave-bosons $\Phi(E_\Gamma; 2q)$ for each local multiplets $|\Gamma\rangle$.

using the symmetry adapted basis. The procedure can be found in Ref. [89]. On the other hand, for the pairing state, we construct the many-body variational basis following the procedure in Ref. [62]. First, since the Hubbard-Kanamori interaction (Eq. (3)) can be written into

$$H_{\text{loc}} = (U - 3J) \frac{\hat{N}(\hat{N} - 1)}{2} - J \left[2\hat{\mathbf{S}}^2 + \frac{1}{2}\hat{\mathbf{L}}^2 \right] + \frac{5}{2}J\hat{N} \quad (\text{C1})$$

with

$$\hat{L}_\alpha = \sum_{\beta\gamma\sigma} \hat{d}_{i\beta\sigma}^\dagger [-i\epsilon_{\alpha\beta\gamma}] \hat{d}_{i\gamma\sigma} \quad (\text{C2})$$

$$\hat{\mathbf{S}} = \frac{1}{2} \sum_{\alpha\sigma\sigma'} \hat{d}_{i\alpha\sigma}^\dagger \boldsymbol{\sigma}_{\sigma\sigma'} \hat{d}_{i\alpha\sigma'} \quad (\text{C3})$$

$$\hat{N} = \sum_{\alpha\sigma} \hat{d}_{i\alpha\sigma}^\dagger \hat{d}_{i\alpha\sigma}, \quad (\text{C4})$$

the local Hamiltonian is diagonalized in the $\Gamma = (N, L, S)$ basis. The $\boldsymbol{\sigma}$ is a vector of Pauli matrices, and $\epsilon_{\alpha\beta\gamma}$ is the Levi-Civita symbol, which can be expressed in terms of Gell-Mann matrices λ^4 , λ^5 , and λ^6 . Therefore, the slave-boson amplitude can be significantly reduced to

$$\begin{aligned} \Phi_{\Gamma n} = & \langle \Gamma | n \rangle \Phi(E_\Gamma) + \sum_{q=1}^3 \left[\frac{\langle n | (\hat{\mathcal{O}}_P)^q | \Gamma \rangle}{\sqrt{\langle \Gamma | (\hat{\mathcal{O}}_P^\dagger)^q (\hat{\mathcal{O}}_P)^q | \Gamma \rangle}} \Phi(E_\Gamma; 2q), \right. \\ & \left. + \frac{\langle n | (\hat{\mathcal{O}}_P^\dagger)^q | \Gamma \rangle}{\sqrt{\langle \Gamma | (\hat{\mathcal{O}}_P)^q (\hat{\mathcal{O}}_P^\dagger)^q | \Gamma \rangle}} \Phi(E_\Gamma; -2q) \right] \quad (\text{C5}) \end{aligned}$$

where E_Γ and $|\Gamma\rangle$ is the eigenvalue and the eigenstate of Eq. (C1), respectively. Comparing Eq. (C5) to Eq. (B16), we identify that the many-body basis for the normal state part is

$$\phi_p = \langle \Gamma | n \rangle,$$

with the corresponding slave-boson $c_p = \Phi(E_\Gamma)$, and the pairing part are

$$\phi_p = \frac{\langle n | (\hat{\mathcal{O}}_P)^q | \Gamma \rangle}{\sqrt{\langle \Gamma | (\hat{\mathcal{O}}_P^\dagger)^q (\hat{\mathcal{O}}_P)^q | \Gamma \rangle}}$$

and

$$\phi_p = \frac{\langle n | (\hat{\mathcal{O}}_P^\dagger)^q | \Gamma \rangle}{\sqrt{\langle \Gamma | (\hat{\mathcal{O}}_P)^q (\hat{\mathcal{O}}_P^\dagger)^q | \Gamma \rangle}}$$

with the corresponding slave-boson amplitudes $c_p = \Phi(E_\Gamma; 2q)$ and $c_p = \Phi(E_\Gamma; -2q)$, respectively. In the end, we have 43 bosonic amplitudes listed in Tab. I.

2. Single-particle basis

The single-particle basis \mathbf{h}_s and $\tilde{\mathbf{h}}_s$, parameterizing Eqs. (B11)-(B15), are block matrices,

$$\mathbf{h}_s = \begin{pmatrix} h_s & h'_s \\ h'_s{}^\dagger & -h_s^* \end{pmatrix}, \quad \tilde{\mathbf{h}}_s = \begin{pmatrix} h_s & h'_s{}^* \\ h'_s & h_s^* \end{pmatrix}, \quad (\text{C6})$$

where the component h_s corresponds to the normal part and h'_s corresponds to the anomalous part of the matrix. The components for each fluctuation channel, in the degenerate three-orbital model, are as follow:

$$h_{\text{ch}} = \lambda_0 \otimes \sigma_0, \quad (\text{C7})$$

$$h_{\text{sp}} = \lambda_0 \otimes \sigma_z, \quad (\text{C8})$$

$$h_{\text{orb}} = \lambda_4 \otimes \sigma_0, \quad (\text{C9})$$

$$h_{\text{so}} = \lambda_4 \otimes \sigma_z, \quad (\text{C10})$$

$$h_{\text{orb}^*} = \lambda_1 \otimes \sigma_0, \quad (\text{C11})$$

$$h_{\text{so}^*} = \lambda_1 \otimes \sigma_z, \quad (\text{C12})$$

$$h_{\text{P}} = 0, \quad (\text{C13})$$

for the normal part, and

$$h'_{\text{ch}} = h'_{\text{sp}} = h'_{\text{orb}} = h'_{\text{so}} = h'_{\text{orb}^*} = h'_{\text{so}^*} = 0 \quad (\text{C14})$$

$$h'_{\text{P}} = \lambda_6 \otimes [-i\sigma_y\sigma_z] \quad (\text{C15})$$

for the anomalous part, where the basis is chosen to be normalized, i.e., $\text{Tr}[\mathbf{h}_s \mathbf{h}_s^\dagger] = 1$. We see that \mathbf{h}_{P} describes the pairing fluctuation, while \mathbf{h}_{ch} , \mathbf{h}_{sp} , \mathbf{h}_{orb} , \mathbf{h}_{so} , $\mathbf{h}_{\text{orb}^*}$, and \mathbf{h}_{so^*} describes the charge, spin, orbital, and spin-orbital fluctuations, respectively.

Appendix D: Derivation of Eq. (37)

The linear response for a generic operator is given by the following equation:

$$\begin{aligned} \chi_{\mathcal{O}\mathcal{O}} &= \frac{d}{d\xi} \langle \Phi(\xi, \mathbf{x}) | \hat{\mathcal{O}} | \Phi(\xi, \mathbf{x}) \rangle \Big|_{(\xi=0, \mathbf{x}(\xi=0))} \\ &= \chi_{\mathcal{O}\mathcal{O}}^{(0)} + \sum_{\mu} \frac{dx_{\mu}}{d\xi} \Big|_{\xi=0} \chi_{\mu\mathcal{O}}. \end{aligned} \quad (\text{D1})$$

Note again that μ runs through all the variational variables in \mathbf{x} (Eq. (26)), and we use the variational parameters as the subscripts. To evaluate Eq. (D1), it is necessary to calculate $\frac{dx_{\mu}}{d\xi} \Big|_{\xi=0}$, which can be determined by taking the total derivative of Eq. (36) with respect to ξ , as follows:

$$\sum_{\nu} \mathcal{M}_{\mu\nu} \frac{dx_{\nu}}{d\xi} \Big|_{\xi=0} - \chi_{\mu\mathcal{O}} = 0, \quad (\text{D2})$$

where \mathcal{M} is the fluctuation matrix defined in Eq. (40). Substituting Eq. (D2) into Eq. (D1), we obtain Eq. (37) in the main text. Since physical susceptibilities in Eq. (53) are gauge invariant, all solutions of Eq. (D2), connected by the gauge transformations (Eq. (H6)), are equivalent.

Appendix E: Fluctuation Matrix

The fluctuation matrix can be separated into three parts:

$$\mathcal{M}_{\mu\nu}(\mathbf{q}) = \mathcal{M}_{\mu\nu}^{\text{mix}} + \mathcal{M}_{\mu\nu}^{\text{qp}}(\mathbf{q}) + \mathcal{M}_{\mu\nu}^{\text{emb}} \quad (\text{E1})$$

The first part \mathcal{M}^{mix} , which involves the partial derivatives of the mixing term of the Lagrangian \mathcal{L}_{mix} with respect to r_s , l_s , d_s , D_s , l_s^c , and ζ_s , is computed from the following equations:

$$\begin{aligned} \mathcal{M}_{r_s d_s'}^{\text{mix}} &\equiv \partial_{r_s} \partial_{d_s'} \mathcal{L}_{\text{mix}}[\mathbf{x}] \Big|_{(\xi=0, \mathbf{x}(\xi=0))} = - \sum_{a\alpha c} (\mathbf{D}_{a\alpha} \tilde{\mathbf{h}}_{s,c\alpha} \\ &\partial_{d_s'} [\mathbf{\Delta}(1 - \mathbf{\Delta})]_{ca}^{\frac{1}{2}} + \text{c.c.}), \end{aligned} \quad (\text{E2})$$

$$\begin{aligned} \mathcal{M}_{r_s D_s'}^{\text{mix}} &\equiv \partial_{r_s} \partial_{D_s'} \mathcal{L}_{\text{mix}}[\mathbf{x}] \Big|_{(\xi=0, \mathbf{x}(\xi=0))} = - \sum_{a\alpha c} (\tilde{\mathbf{h}}_{s,a\alpha} \tilde{\mathbf{h}}_{s',c\alpha} \\ &[\mathbf{\Delta}(1 - \mathbf{\Delta})]_{ca}^{\frac{1}{2}} + \text{c.c.}), \end{aligned} \quad (\text{E3})$$

$$\mathcal{M}_{l_s d_s'}^{\text{mix}} = \mathcal{M}_{d_s l_s'}^{\text{mix}} = \mathcal{M}_{d_s \zeta_s'}^{\text{mix}} = -\frac{1}{2} \sum_{ab} \mathbf{h}_{ab}^s [\mathbf{h}^{s'}]_{ab}^t, \quad (\text{E4})$$

$$\begin{aligned} \mathcal{M}_{d_s d_s'}^{\text{mix}} &\equiv \partial_{d_s} \partial_{d_s'} \mathcal{L}_{\text{mix}}[\mathbf{x}] \Big|_{(\xi=0, \mathbf{x}(\xi=0))} = - \sum_{a\alpha c} (\mathbf{D}_{a\alpha} \mathbf{R}_{c\alpha} \\ &\partial_{d_s} \partial_{d_s'} [\mathbf{\Delta}(1 - \mathbf{\Delta})]_{ca}^{\frac{1}{2}} + \text{c.c.}), \end{aligned} \quad (\text{E5})$$

$$\begin{aligned} \mathcal{M}_{d_s D_s'}^{\text{mix}} &\equiv \partial_{d_s} \partial_{D_s'} \mathcal{L}_{\text{mix}}[\mathbf{x}] \Big|_{(\xi=0, \mathbf{x}(\xi=0))} = - \sum_{a\alpha c} (\tilde{\mathbf{h}}_{s',a\alpha} \mathbf{R}_{c\alpha} \\ &\partial_{d_s} [\mathbf{\Delta}(1 - \mathbf{\Delta})]_{ca}^{\frac{1}{2}} + \text{c.c.}), \end{aligned} \quad (\text{E6})$$

and the other unlisted components of \mathcal{M}^{mix} are zero.

The second part \mathcal{M}^{qp} , which involves the partial derivatives of the quasiparticle term of the Lagrangian \mathcal{L}_{qp} with respect to r_s and l_s , is computed from the following equations:

$$\begin{aligned} \mathcal{M}_{r_s r_s'}^{\text{qp}}(q) &= \partial_{r_s, -q} \partial_{r_s', q} \mathcal{L}_{\text{qp}}[\mathbf{x}] \Big|_{(\xi=0, \mathbf{x}(\xi=0))} \\ &= \frac{1}{2N} \sum_{\mathbf{k}} \text{Tr} \left\{ n_F(H_{\mathbf{k}}^{\text{qp}}) \left[\tilde{\mathbf{h}}_s \tilde{\mathbf{\epsilon}}_{\mathbf{k}+\mathbf{q}} \tilde{\mathbf{h}}_{s'}^\dagger + \tilde{\mathbf{h}}_{s'} \tilde{\mathbf{\epsilon}}_{\mathbf{k}-\mathbf{q}} \tilde{\mathbf{h}}_s^\dagger \right] \right. \\ &+ T \sum_{\omega_n} \mathbf{G}_k[\mathbf{R}]^{-1} [\mathbf{R} \tilde{\mathbf{\epsilon}}_{\mathbf{k}} \tilde{\mathbf{h}}_s^\dagger + \tilde{\mathbf{h}}_s \tilde{\mathbf{\epsilon}}_{\mathbf{k}+\mathbf{q}} \mathbf{R}^\dagger] [\mathbf{R}^\dagger]^{-1} \mathbf{G}_{k+q} \\ &\cdot [\mathbf{R}]^{-1} [\mathbf{R} \tilde{\mathbf{\epsilon}}_{\mathbf{k}+\mathbf{q}} \tilde{\mathbf{h}}_{s'}^\dagger + \tilde{\mathbf{h}}_{s'} \tilde{\mathbf{\epsilon}}_{\mathbf{k}} \mathbf{R}^\dagger] [\mathbf{R}^\dagger]^{-1} \left. \right\}, \end{aligned} \quad (\text{E7})$$

$$\begin{aligned} \mathcal{M}_{r_s l_s'}^{\text{qp}}(q) &\equiv \partial_{r_s, -q} \partial_{l_s', q} \mathcal{L}_{\text{qp}}[\mathbf{x}] \Big|_{(\xi=0, \mathbf{x}(\xi=0))} \\ &= \frac{T}{2N} \sum_k \text{Tr} \left\{ \mathbf{G}_k[\mathbf{R}]^{-1} \left[\mathbf{R} \tilde{\mathbf{\epsilon}}_{\mathbf{k}} \tilde{\mathbf{h}}_s^\dagger + \tilde{\mathbf{h}}_s \tilde{\mathbf{\epsilon}}_{\mathbf{k}+\mathbf{q}} \mathbf{R}^\dagger \right] \right. \\ &\cdot [\mathbf{R}^\dagger]^{-1} \mathbf{G}_{k+q} [\mathbf{R}]^{-1} \mathbf{h}_{s'} [\mathbf{R}^\dagger]^{-1} \left. \right\}, \end{aligned} \quad (\text{E8})$$

$$\begin{aligned}
\mathcal{M}_{l_s l_{s'}}^{\text{qp}}(q) &\equiv \partial_{l_s, -q} \partial_{l_{s'}, q} \mathcal{L}_{\text{qp}}[\mathbf{x}] \Big|_{(\xi=0, \mathbf{x}(\xi=0))} \\
&= \frac{T}{2N} \sum_k \text{Tr} \left\{ \mathbf{G}_k[\mathbf{R}]^{-1} \mathbf{h}_s[\mathbf{R}^\dagger]^{-1} \right. \\
&\quad \left. \cdot \mathbf{G}_{k+q}[\mathbf{R}]^{-1} \mathbf{h}_{s'}[\mathbf{R}^\dagger]^{-1} \right\}, \quad (\text{E9})
\end{aligned}$$

and the other unlisted components of \mathcal{M}^{qp} are zero. We also defined $k = (\omega_n, \mathbf{k})$ and $\sum_k \equiv \sum_{\mathbf{k}} \sum_{\omega_n}$. Note that since we consider degenerate three-orbital model, at the normal-state saddle-point, the renormalization matrix, the local potential, the quasiparticle energy dispersion, and the Green's functions are all degenerate and diagonal matrices, i.e.,

$$\mathbf{R} = R_0 \begin{pmatrix} I & 0 \\ 0 & I \end{pmatrix}, \quad (\text{E10})$$

$$\mathbf{\Lambda} = l_0 \begin{pmatrix} I & 0 \\ 0 & -I \end{pmatrix}, \quad (\text{E11})$$

$$H_{\mathbf{k}}^{\text{qp}} = E_{\mathbf{k}}^{\text{qp}} \begin{pmatrix} I & 0 \\ 0 & -I \end{pmatrix} \quad (\text{E12})$$

$$\mathbf{G}^{\text{qp}}(k) = \begin{pmatrix} \frac{1}{i\omega_n - E_{\mathbf{k}}^{\text{qp}}} I & 0 \\ 0 & \frac{1}{-i\omega_n - E_{\mathbf{k}}^{\text{qp}}} I \end{pmatrix}, \quad (\text{E13})$$

where $E_{\mathbf{k}}^{\text{qp}} = R_0^2 \epsilon_{\mathbf{k}} + l_0$ and I is the 6×6 identity matrix. The Matsubara summation for the fermionic Green's function convolutions in $\mathcal{M}_{rr}^{\text{qp}}$, $\mathcal{M}_{rl}^{\text{qp}}$, and $\mathcal{M}_{ll}^{\text{qp}}$

can be evaluated analytically from the Lindhard function. For example, the particle-hole convolution:

$$\begin{aligned}
T \sum_{\omega_m} \frac{1}{i\omega_m - E_{\mathbf{k}}^{\text{qp}}} \frac{1}{i\omega_m + i\Omega_n - E_{\mathbf{k}+\mathbf{q}}^{\text{qp}}} \\
= \frac{n_F(E_{\mathbf{k}}^{\text{qp}}) - n_F(E_{\mathbf{k}+\mathbf{q}}^{\text{qp}})}{i\Omega_n - E_{\mathbf{k}+\mathbf{q}}^{\text{qp}} + E_{\mathbf{k}}^{\text{qp}}}. \quad (\text{E14})
\end{aligned}$$

and the particle-particle convolution:

$$\begin{aligned}
T \sum_{\omega_m} \frac{1}{i\omega_m + i\Omega_n - E_{\mathbf{k}+\mathbf{q}}^{\text{qp}}} \frac{1}{-i\omega_m - E_{-\mathbf{k}}^{\text{qp}}} \\
= \frac{n_F(E_{\mathbf{k}+\mathbf{q}}^{\text{qp}}) - n_F(-E_{-\mathbf{k}}^{\text{qp}})}{i\Omega_n - E_{\mathbf{k}+\mathbf{q}}^{\text{qp}} - E_{-\mathbf{k}}^{\text{qp}}}, \quad (\text{E15})
\end{aligned}$$

The analytical continuation to real frequency can be achieved by replacing $i\Omega_n \rightarrow \omega + i0^+$.

The third part \mathcal{M}^{emb} involves the partial derivatives of the embedding term of the Lagrangian \mathcal{L}_{emb} with respect to D_s , l_s^c , and ζ_s , which can be evaluated as follows. First, we evaluate the first order derivatives using the Hellmann-Feynman theorem:

$$\partial_{l_s^c} \mathcal{L}_{\text{emb}}[\xi, \mathbf{x}] = \sum_{abcd} \frac{1}{2} \mathbf{h}_{ab}^s \langle \Phi(\xi, \mathbf{x}) | \bar{I}_{bc} \hat{\Psi}_c \hat{\Psi}_d^\dagger \bar{I}_{da} | \Phi(\xi, \mathbf{x}) \rangle, \quad (\text{E16})$$

$$\partial_{D_s} \mathcal{L}_{\text{emb}}[\xi, \mathbf{x}] = 2 \sum_{aab} \tilde{\mathbf{h}}_{a\alpha}^s \langle \Phi(\xi, \mathbf{x}) | \hat{\Xi}_\alpha^\dagger \hat{\Psi}_b \bar{I}_{ba} | \Phi(\xi, \mathbf{x}) \rangle, \quad (\text{E17})$$

$$\partial_{\zeta_s} \mathcal{L}_{\text{emb}}[\xi, \mathbf{x}] = \frac{1}{2} \sum_{\alpha\beta} \mathbf{h}_{\alpha\beta}^s \langle \Phi(\xi, \mathbf{x}) | \hat{\Xi}_\alpha^\dagger \hat{\Xi}_\beta | \Phi(\xi, \mathbf{x}) \rangle. \quad (\text{E18})$$

Then, we can compute the second order derivatives from the following equations:

$$\mathcal{M}_{l_s^c l_{s'}^c}^{\text{emb}} = \partial_{l_s^c} \partial_{l_{s'}^c} \mathcal{L}_{\text{emb}}[\xi, \mathbf{x}] \Big|_{(\xi=0, \mathbf{x}(\xi=0))} = \partial_{l_s^c} \sum_{abcd} \frac{1}{2} \mathbf{h}_{ab}^{s'} \langle \Phi(\xi, \mathbf{x}) | \bar{I}_{bc} \hat{\Psi}_c \hat{\Psi}_d^\dagger \bar{I}_{da} | \Phi(\xi, \mathbf{x}) \rangle \Big|_{(\xi=0, \mathbf{x}(\xi=0))}, \quad (\text{E19})$$

$$\mathcal{M}_{D_s D_{s'}}^{\text{emb}} = \partial_{l_s^c} \partial_{D_{s'}} \mathcal{L}_{\text{emb}}[\xi, \mathbf{x}] \Big|_{(\xi=0, \mathbf{x}(\xi=0))} = \partial_{l_s^c} 2 \sum_{aab} \tilde{\mathbf{h}}_{a\alpha}^{s'} \langle \Phi(\xi, \mathbf{x}) | \hat{\Xi}_\alpha^\dagger \hat{\Psi}_b \bar{I}_{ba} | \Phi(\xi, \mathbf{x}) \rangle \Big|_{(\xi=0, \mathbf{x}(\xi=0))}, \quad (\text{E20})$$

$$\mathcal{M}_{D_s l_{s'}^c}^{\text{emb}} = \partial_{D_s} \partial_{l_{s'}^c} \mathcal{L}_{\text{emb}}[\xi, \mathbf{x}] \Big|_{(\xi=0, \mathbf{x}(\xi=0))} = \partial_{D_s} \frac{1}{2} \sum_{abcd} \mathbf{h}_{ab}^{s'} \langle \Phi(\xi, \mathbf{x}) | \bar{I}_{bc} \hat{\Psi}_c \hat{\Psi}_d^\dagger \bar{I}_{da} | \Phi(\xi, \mathbf{x}) \rangle \Big|_{(\xi=0, \mathbf{x}(\xi=0))}, \quad (\text{E21})$$

$$\mathcal{M}_{D_s D_{s'}}^{\text{emb}} = \partial_{D_s} \partial_{D_{s'}} \mathcal{L}_{\text{emb}}[\xi, \mathbf{x}] \Big|_{(\xi=0, \mathbf{x}(\xi=0))} = \partial_{D_s} 2 \sum_{aab} \tilde{\mathbf{h}}_{a\alpha}^{s'} \langle \Phi(\xi, \mathbf{x}) | \hat{\Xi}_\alpha^\dagger \hat{\Psi}_b \bar{I}_{ba} | \Phi(\xi, \mathbf{x}) \rangle \Big|_{(\xi=0, \mathbf{x}(\xi=0))}, \quad (\text{E22})$$

$$\mathcal{M}_{D_s \zeta_{s'}}^{\text{emb}} = \partial_{l_s^c} \partial_{\zeta_{s'}} \mathcal{L}_{\text{emb}}[\xi, \mathbf{x}] \Big|_{(\xi=0, \mathbf{x}(\xi=0))} = \partial_{D_s} \frac{1}{2} \sum_{\alpha\beta} \mathbf{h}_{\alpha\beta}^{s'} \langle \Phi(\xi, \mathbf{x}) | \hat{\Xi}_\alpha^\dagger \hat{\Xi}_\beta | \Phi(\xi, \mathbf{x}) \rangle \Big|_{(\xi=0, \mathbf{x}(\xi=0))}, \quad (\text{E23})$$

$$\mathcal{M}_{\zeta_s, l_s^c}^{\text{emb}} = \partial_{\zeta_s} \partial_{l_s^c} \mathcal{L}_{\text{emb}}[\xi, \mathbf{x}] \Big|_{(\xi=0, \mathbf{x}(\xi=0))} = \partial_{\zeta_s} \frac{1}{2} \sum_{abcd} \mathbf{h}_{ab}^{s'} \langle \Phi(\xi, \mathbf{x}) | \bar{I}_{bc} \hat{\Psi}_c \hat{\Psi}_d^\dagger \bar{I}_{da} | \Phi(\xi, \mathbf{x}) \rangle \Big|_{(\xi=0, \mathbf{x}(\xi=0))}, \quad (\text{E24})$$

$$\mathcal{M}_{\zeta_s D_s'}^{\text{emb}} = \partial_{\zeta_s} \partial_{D_s'} \mathcal{L}_{\text{emb}}[\xi, \mathbf{x}] \Big|_{(\xi=0, \mathbf{x}(\xi=0))} = \partial_{\zeta_s} 2 \sum_{aab} \tilde{\mathbf{h}}_{a\alpha}^{s'} \langle \Phi(\xi, \mathbf{x}) | \hat{\Xi}_\alpha^\dagger \hat{\Psi}_b \bar{I}_{ba} | \Phi(\xi, \mathbf{x}) \rangle \Big|_{(\xi=0, \mathbf{x}(\xi=0))}, \quad (\text{E25})$$

$$\mathcal{M}_{\zeta_s \zeta_{s'}}^{\text{emb}} = \partial_{\zeta_s} \partial_{\zeta_{s'}} \mathcal{L}_{\text{emb}}[\xi, \mathbf{x}] \Big|_{(\xi=0, \mathbf{x}(\xi=0))} = \partial_{\zeta_s} \frac{1}{2} \sum_{\alpha\beta} \mathbf{h}_{\alpha\beta}^{s'} \langle \Phi(\xi, \mathbf{x}) | \hat{\Xi}_\alpha^\dagger \hat{\Xi}_\beta | \Phi(\xi, \mathbf{x}) \rangle \Big|_{(\xi=0, \mathbf{x}(\xi=0))}, \quad (\text{E26})$$

where the other unlisted components of \mathcal{M}^{emb} are zero.

The above second-order derivatives and Eqs. (38)-(39) can be evaluated using the linear response theory. We apply a perturbation to the embedding Hamiltonian

$$\hat{H}_{\text{emb}}(\eta) = \hat{H}_{\text{emb}} + \eta \hat{A}, \quad (\text{E27})$$

where $\hat{A} = \sum_{abcd} \mathbf{h}_{ab}^s \bar{I}_{bc} \hat{\Psi}_c \hat{\Psi}_d^\dagger \bar{I}_{da}$, $\sum_{aab} \tilde{\mathbf{h}}_{a\alpha}^s \hat{\Xi}_\alpha^\dagger \hat{\Psi}_b \bar{I}_{ba}$, or \hat{O} corresponding to the perturbation in $\eta = l_s^c$, D_s , or ξ , respectively. We want to compute the change in the average of $\langle \hat{B} \rangle_\eta$ in the limit $\eta \rightarrow 0$, where $\hat{B} = \sum_{abcd} \mathbf{h}_{ab}^s \bar{I}_{bc} \hat{\Psi}_c \hat{\Psi}_d^\dagger \bar{I}_{da}$, $\sum_{aab} \tilde{\mathbf{h}}_{a\alpha}^s \hat{\Xi}_\alpha^\dagger \hat{\Psi}_b \bar{I}_{ba}$, or \hat{O} . This response function can be computed from the spectral representation of the static susceptibility at zero temperature:

$$\begin{aligned} \left. \frac{\partial \langle \hat{B} \rangle_\eta}{\partial \eta} \right|_{\eta=0} &= \chi_{\hat{A}\hat{B}} \\ &= \lim_{\epsilon \rightarrow 0^+} \sum_n \left[\frac{\langle 0 | \hat{A} | n \rangle \langle n | \hat{B} | 0 \rangle}{E_n - E_0 + i\epsilon} - \frac{\langle 0 | \hat{B} | n \rangle \langle n | \hat{A} | 0 \rangle}{E_0 - E_n + i\epsilon} \right], \quad (\text{E28}) \end{aligned}$$

where E_n is the n -th excited state energy of \hat{H}_{emb} and $|n\rangle$ is the n -th excited state wavefunction of \hat{H}_{emb} .

Beside the method proposed in Eqs. (E28), one can also use the finite difference method to evaluate the partial derivatives in Eqs. (E19)-(E26). Note that both methods requires the diagonalization of the embedding Hamiltonian \hat{H}_{emb} , which is the most time-consuming part of the linear-response calculations. With the current state-of-the-art, we can easily study the f -electron materials, containing 7 correlated orbitals, using exact-diagonalization and machine learning techniques [90]. For the systems with more correlated orbital, one may also utilize the density matrix renormalization group or auxiliary-field quantum Monte Carlo methods [91].

Appendix F: Fluctuation matrix as a bosonic propagator

Here we discuss how the fluctuation matrix can be interpreted as the propagator for the fluctuations of the

bosonic variables \mathbf{x}_i . Let us expand the Lagrangian, Eq. (46), to the second order in

$$\begin{aligned} \delta \mathbf{x}_i^t &= (\delta r_{\text{ch}}, \delta l_{\text{ch}}, \delta d_{\text{ch}}, \delta D_{\text{ch}}, \delta l_s^c, \delta \zeta_{\text{ch}}, \dots, \delta r_s, \delta l_s, \delta d_s, \\ &\quad \delta D_s, \delta l_s^c, \delta \zeta_s, \dots, \delta r_{\text{P}}, \delta l_{\text{P}}, \delta d_{\text{P}}, \delta D_{\text{P}}, \delta l_{\text{P}}^c, \delta \zeta_{\text{P}}) \end{aligned} \quad (\text{F1})$$

around the normal-state saddle-point:

$$\begin{aligned} \mathcal{L}^s[\delta \mathbf{x}, \Xi, \Xi^\dagger] &= \frac{T}{2N} \sum_k \sum_{\alpha\beta} \Xi_{\mathbf{k}\alpha}^\dagger [\mathbf{G}(k)]_{\alpha\beta}^{-1} \Xi_{\mathbf{k}\beta} \\ &+ \frac{1}{2} \sum_i \delta \mathbf{x}_i^t \left[\mathcal{M}^{\text{mix}} + \mathcal{M}^{\text{emb}} \right] \delta \mathbf{x}_i \\ &+ \sum_{\mathbf{k}, \mathbf{q}} \sum_{\alpha\beta} \left[(\tilde{\Lambda}_{\alpha\beta, r_s}^{\mathbf{k}, \mathbf{q}} \delta r_{s, \mathbf{q}} \Xi_{\mathbf{k}+\mathbf{q}\alpha}^\dagger \Xi_{\mathbf{k}\beta} \right. \\ &+ \text{h.c.}) + \tilde{\Lambda}_{\alpha\beta, l_s} \delta l_{s, \mathbf{q}} \Xi_{\mathbf{k}+\mathbf{q}\alpha}^\dagger \Xi_{\mathbf{k}\beta} \left. \right] \\ &+ \sum_{\mathbf{k}, \mathbf{k}', \mathbf{q}} \sum_{\alpha\beta} \tilde{\gamma}_{\alpha\beta, r_s r_{s'}}^{\mathbf{k}, \mathbf{k}', \mathbf{q}} \delta r_{s, \mathbf{q}} \delta r_{s', -\mathbf{q}} \Xi_{\mathbf{k}\alpha}^\dagger \Xi_{\mathbf{k}'\beta}, \quad (\text{F2}) \end{aligned}$$

where $\tilde{\Lambda}_{\alpha\beta\mu}$ are the three-leg vertices defined in Eq. (60) and (61) and $\mathbf{G}(k)$ is the Nambu propagator. We also introduce the four-leg vertex:

$$\tilde{\gamma}_{\alpha\beta r_s r_{s'}}^{\mathbf{k}, \mathbf{k}', \mathbf{q}} = \frac{1}{2} \left[\mathbf{R}^{-1} (\tilde{\mathbf{h}}_s \tilde{\mathbf{e}}_{\mathbf{k}+\mathbf{q}} \tilde{\mathbf{h}}_{s'}^\dagger + \tilde{\mathbf{h}}_{s'} \tilde{\mathbf{e}}_{\mathbf{k}'-\mathbf{q}} \tilde{\mathbf{h}}_s^\dagger) (\mathbf{R}^\dagger)^{-1} \right]_{\alpha\beta}. \quad (\text{F3})$$

We immediately see that the \mathbf{q} independent part of the fluctuation matrix:

$$\mathcal{M}^{\text{mix}} + \mathcal{M}^{\text{emb}} \equiv \mathcal{D}_0^{-1} \quad (\text{F4})$$

can be viewed, in the Gaussian fluctuation sense [38], as the inverse of the bare bosonic propagator \mathcal{D}_0^{-1} . It is important to note that \mathcal{D}_0 describes the local multiplet fluctuations because it contains the embedding susceptibilities shown in Eqs. (E19)-(E26). We see that, for the pairing channel $s = \text{P}$ in Eqs. (E19)-(E26), the multiplet fluctuation selects the basis \mathbf{h}_{P} that increases and removes electron pairs from the saddle-point wavefunction. Therefore, it describes the local fluctuation with pair excitations. On the other hand, for channel $s \in \{\text{ch}, \text{sp}, \text{orb}, \text{so}, \text{orb}^*, \text{so}^*\}$, the particle number is conserved. Consequently, they describe the corresponding local charge, orbital, and spin fluctuations.

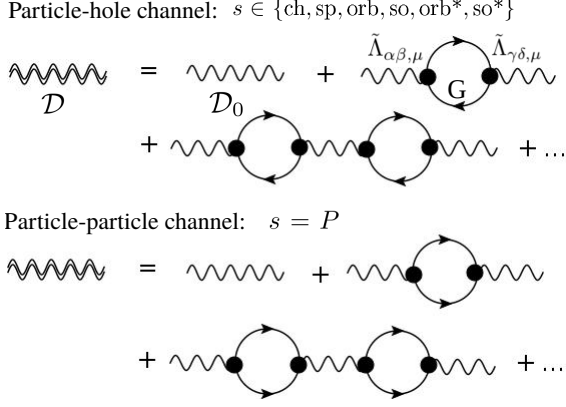


Figure 8. Diagrammatic representation of the Dyson equation in Eq. (F5). The double wavy line and the wavy line denotes the dressed bosonic propagator \mathcal{D} and the bare bosonic propagator \mathcal{D}_0 . The solid line denotes the Nambu propagator \mathbf{G} . The circle denotes the three-leg vertices $\tilde{\Lambda}$.

We now discuss the role of $\mathcal{M}^{\text{qp}}(\mathbf{q})$. By integrating out the fermionic field $\Xi_{\mathbf{k}\alpha}$ in Eq. (F2) to the one-loop order, we found the self-energy correction is related to the fluctuation matrix through $\pi(\mathbf{q}) \equiv -\mathcal{M}^{\text{qp}}(\mathbf{q})$. Therefore, we can write the total fluctuation matrix in terms of the Dyson equation:

$$\mathcal{M}(\mathbf{q}) \equiv \mathcal{D}^{-1}(\mathbf{q}) = \mathcal{D}_0^{-1} - \pi(\mathbf{q}). \quad (\text{F5})$$

The total fluctuation matrix corresponds to the dressed bosonic propagator with the self-energy correction summing the fermionic bubbles to the infinite order. From Eq. (E7)-(E9), we see that \mathcal{M}^{qp} contains only the particle-particle bubbles for the pairing channel $s = P$, and the particle-hole bubbles for the other channels $s \in \{\text{ch, sp, orb, so, orb}^*, \text{so}^*\}$. Figure 8 shows the diagrammatic representation of the Dyson equation for the particle-hole and the particle-particle channels.

Appendix G: Random phase approximation for the interaction vertex

In this section, we derive the random phase approximation for the interaction vertex at $\mathbf{q} = 0$. Therefore, we suppress the \mathbf{q} dependent of $\tilde{\Gamma}$, $\tilde{\lambda}$, \mathcal{D} , and π in the following derivation. The interaction vertex has the following form (see Eqs. (64) and (F5)):

$$\begin{aligned} \tilde{\Gamma}_{\alpha\beta\gamma\delta}^s(\mathbf{k}, \mathbf{k}') = & -4 \left[\tilde{\Lambda}_{\alpha\beta r_s}(\mathbf{k}) \mathcal{D}_{r_s r_s} \tilde{\Lambda}_{\gamma\delta r_s}(\mathbf{k}') \right. \\ & \left. + 2\tilde{\Lambda}_{\alpha\beta r_s}(\mathbf{k}) \tilde{\Lambda}_{\gamma\delta l_s}(\mathbf{k}') \mathcal{D}_{r_s l_s} + \tilde{\Lambda}_{\alpha\beta l_s}(\mathbf{k}) \tilde{\Lambda}_{\gamma\delta l_s}(\mathbf{k}') \mathcal{D}_{l_s l_s} \right], \end{aligned} \quad (\text{G1})$$

where $\tilde{\Lambda}_\mu$ is the three-leg vertex and $\mathcal{D} \equiv \mathcal{M}^{-1}$ is the bosonic Green's function defined in Eq. (F5). We want

to obtain an RPA like form for the vertex:

$$\tilde{\Gamma}_{\alpha\beta\gamma\delta}^s \equiv \langle \langle \tilde{\Gamma}_{\alpha\beta\gamma\delta}^s(\mathbf{k}, \mathbf{k}') \rangle \rangle_{\mathbf{k}_F} \mathbf{k}'_F = \frac{F_s}{1 + F_s \chi_{\mathcal{O}_s \mathcal{O}_s}^{(0)}} [\mathbf{h}_s]_{\alpha\beta} [\mathbf{h}_s]_{\gamma\delta}, \quad (\text{G2})$$

after averaging \mathbf{k} and \mathbf{k}' over the Fermi surface, where F_s is the Landau parameter.

We know that the bosonic Green's function has the following Dyson form for each sector s (see Eq. (F5)):

$$\mathcal{D}_s = \left[[\mathcal{D}_{0,s}]^{-1} - \pi_s \right]^{-1} \quad (\text{G3})$$

$$= \left[1 - \mathcal{D}_{0,s} \pi \right]^{-1} \mathcal{D}_{0,s}, \quad (\text{G4})$$

where \mathcal{D}_0 is the bare bosonic propagator, and the self-energy in each sector s has the form

$$\pi_s = \begin{pmatrix} \pi_{r_s r_s} & \pi_{r_s l_s} & 0 & 0 & 0 & 0 \\ \pi_{r_s l_s} & \pi_{l_s l_s} & 0 & 0 & 0 & 0 \\ 0 & 0 & 0 & 0 & 0 & 0 \\ 0 & 0 & 0 & 0 & 0 & 0 \\ 0 & 0 & 0 & 0 & 0 & 0 \\ 0 & 0 & 0 & 0 & 0 & 0 \end{pmatrix}. \quad (\text{G5})$$

The divergence of \mathcal{D} can be determined from

$$\begin{aligned} \text{Det} \left[1 - \mathcal{D}_{0,s} \pi \right] = & 1 - \mathcal{D}_{0,l_s l_s} \pi_{l_s l_s} - 2\mathcal{D}_{0,r_s l_s} \pi_{r_s l_s} \\ & - \mathcal{D}_{0,r_s r_s} \pi_{r_s r_s} + (\mathcal{D}_{0,r_s l_s} \pi_{r_s l_s})^2 \\ & - \mathcal{D}_{0,l_s l_s} \mathcal{D}_{0,r_s r_s} \pi_{r_s l_s}^2 - (\mathcal{D}_{0,r_s l_s})^2 \pi_{l_s l_s} \pi_{r_s r_s} \\ & + \mathcal{D}_{0,l_s l_s} \mathcal{D}_{0,r_s r_s} \pi_{l_s l_s} \pi_{r_s r_s} = 0. \end{aligned} \quad (\text{G6})$$

The interaction vertex can be expressed in terms of \mathcal{D}_0 , $\tilde{\Lambda}$, and π as

$$\begin{aligned} \tilde{\Gamma}_{\alpha\beta\gamma\delta}^s(\mathbf{k}, \mathbf{k}') = & -\frac{4}{\text{Det} \left[1 - \mathcal{D}_{0,s} \pi \right]} \left[\tilde{\Lambda}_{\alpha\beta r_s}(\mathbf{k}) \tilde{\Lambda}_{\gamma\delta r_s}(\mathbf{k}') \right. \\ & \left(\mathcal{D}_{0,r_s r_s} + (\mathcal{D}_{0,r_s l_s})^2 \pi_{l_s l_s} - \mathcal{D}_{0,l_s l_s} \mathcal{D}_{0,r_s r_s} \pi_{l_s l_s} \right) \\ & + 2\tilde{\Lambda}_{\alpha\beta r_s}(\mathbf{k}) \tilde{\Lambda}_{\gamma\delta l_s}(\mathbf{k}') \left(\mathcal{D}_{0,r_s l_s} - (\mathcal{D}_{0,r_s l_s})^2 \pi_{r_s l_s} \right. \\ & \left. + \mathcal{D}_{0,l_s l_s} \mathcal{D}_{0,r_s r_s} \pi_{r_s l_s} \right) + \tilde{\Lambda}_{\alpha\beta l_s}(\mathbf{k}) \tilde{\Lambda}_{\gamma\delta l_s}(\mathbf{k}') \\ & \left. \left(\mathcal{D}_{0,l_s l_s} + (\mathcal{D}_{0,r_s l_s})^2 \pi_{r_s r_s} - \mathcal{D}_{0,l_s l_s} \mathcal{D}_{0,r_s r_s} \pi_{r_s r_s} \right) \right]. \end{aligned} \quad (\text{G7})$$

We can make further approximation that

$$\begin{aligned} \pi_{r_s r_{s'}} &= \frac{-T}{2N} \sum_k \text{tr} \left\{ \mathbf{G}_k[\mathbf{R}]^{-1} [\mathbf{R} \epsilon_k \tilde{\mathbf{h}}_s^\dagger + \tilde{\mathbf{h}}_s \epsilon_k \mathbf{R}^\dagger] \right. \\ &\quad \left. [\mathbf{R}^\dagger]^{-1} \mathbf{G}_k[\mathbf{R}]^{-1} [\mathbf{R} \epsilon_k \tilde{\mathbf{h}}_{s'}^\dagger + \tilde{\mathbf{h}}_{s'} \epsilon_k \mathbf{R}^\dagger] [\mathbf{R}^\dagger]^{-1} \right\} \Big|_{\xi=0} \\ &\approx 4 \langle \tilde{\Lambda}_r \rangle^2 \chi_{\mathcal{O}_s \mathcal{O}_s}^{(0)}, \end{aligned} \quad (\text{G8})$$

$$\begin{aligned} \pi_{r_s l_{s'}} &= \frac{-T}{2N} \sum_k \text{tr} \left\{ \mathbf{G}_k[\mathbf{R}]^{-1} [\mathbf{R} \epsilon_k \tilde{\mathbf{h}}_s^\dagger + \tilde{\mathbf{h}}_s \epsilon_k \mathbf{R}^\dagger] \right. \\ &\quad \left. [\mathbf{R}^\dagger]^{-1} \mathbf{G}_k[\mathbf{R}]^{-1} \mathbf{h}_{s'} [\mathbf{R}^\dagger]^{-1} \right\} \Big|_{\xi=0} \\ &\approx 4 \langle \tilde{\Lambda}_r \rangle \langle \tilde{\Lambda}_l \rangle \chi_{\mathcal{O}_s \mathcal{O}_s}^{(0)}, \end{aligned} \quad (\text{G9})$$

$$\begin{aligned} \pi_{l_s l_{s'}} &= \frac{-T}{2N} \sum_k \text{tr} \left\{ \mathbf{G}_k[\mathbf{R}]^{-1} \mathbf{h}_{s'} [\mathbf{R}^\dagger]^{-1} \right. \\ &\quad \left. \mathbf{G}_k[\mathbf{R}]^{-1} \mathbf{h}_{s'} [\mathbf{R}^\dagger]^{-1} \right\} \Big|_{\xi=0} \\ &= 4 \langle \tilde{\Lambda}_l \rangle^2 \chi_{\mathcal{O}_s \mathcal{O}_s}^{(0)}, \end{aligned} \quad (\text{G10})$$

where we average the vertex over the Fermi surface:

$$\langle \tilde{\Lambda}_{r_s} \rangle = \frac{R_0^2}{2} \langle 2\epsilon_{\mathbf{k}} \rangle_{\mathbf{k}_F}, \quad (\text{G11})$$

$$\langle \tilde{\Lambda}_{l_s} \rangle = \frac{1}{2}. \quad (\text{G12})$$

We see that, after averaging all the vertices $\tilde{\Lambda}$ and self-energy π in Eq. (G7) over the Fermi surface, there are further cancellation in the denominator and the numerator of $\tilde{\Gamma}^s$ in Eq. (G7). Recasting Eq. (G7) in the form of Eq. (G2), we identify that the irreducible interaction (Landau parameter) F_s in Eq. (G2) for each channel s is

$$F_s = -4 \langle \tilde{\Lambda}_{r_s} \rangle^2 \mathcal{D}_{0, r_s r_s} - 8 \mathcal{D}_{0, r_s l_s} \langle \tilde{\Lambda}_{r_s} \rangle - 4 \mathcal{D}_{0, l_s l_s}. \quad (\text{G13})$$

Appendix H: Gauge invariance

The RISB Lagrangian is invariant under the following gauge transformation [14, 62]:

$$\Phi \rightarrow \Phi U(\theta), \quad \Delta \rightarrow u^t(\theta) \Delta [u^\dagger]^t(\theta), \quad (\text{H1})$$

$$\mathbf{R} \rightarrow u^\dagger(\theta) \mathbf{R}, \quad \Lambda \rightarrow u^\dagger(\theta) \Lambda u(\theta), \quad (\text{H2})$$

$$\mathbf{D} \rightarrow u^t(\theta) \mathbf{D}, \quad \Lambda^c \rightarrow u^\dagger(\theta) \Lambda^c u(\theta), \quad (\text{H3})$$

where

$$u(\theta) = e^{i \sum_s \theta_s \mathbf{T}_{s, ab}}, \quad (\text{H4})$$

$$U(\theta) = e^{i \sum_s \theta_s \mathbf{T}_{s, ab} \Psi_a^\dagger \Psi_b}. \quad (\text{H5})$$

\mathbf{T}_s are the generators for the gauge group, and θ_s are the Lie parameters. The specific form of \mathbf{T}_s corresponding to our variational setup is shown in Appx. I.

We also define the corresponding gauge transformation for \mathbf{x} , see Eq. (26):

$$\mathbf{x} \rightarrow \mathcal{G}_\theta[\mathbf{x}], \quad (\text{H6})$$

where the operator \mathcal{G}_θ transforms each element in Eq. (26) according to Eqs. (H1)-(H3).

Appendix I: Gauge-fixing procedure

In this section, we describe the gauge-fixing procedure for the fluctuation matrix \mathcal{M} . We define a gauge transformation (see Eq. (H6)):

$$\mathbf{x}' = \mathcal{G}_\theta[\mathbf{x}(\xi)] = \mathbf{x}(\xi, \theta(\xi)) \quad (\text{I1})$$

where each component of \mathbf{x} transform as

$$r_s = \text{Tr} [\tilde{\mathbf{h}}_s^\dagger u^\dagger(\theta) \mathbf{R}], \quad l_s = \text{Tr} [\mathbf{h}_s^\dagger u^\dagger(\theta) \Lambda u(\theta)], \quad (\text{I2})$$

$$D_s = \text{Tr} [\tilde{\mathbf{h}}_s^\dagger u^t(\theta) \mathbf{D}], \quad l^c = \text{Tr} [\mathbf{h}_s^\dagger u^\dagger(\theta) \Lambda^c u(\theta)], \quad (\text{I3})$$

$$d_s = \text{Tr} [\mathbf{h}_s^\dagger u^t(\theta) \Delta [u^\dagger]^t(\theta)], \quad (\text{I4})$$

and $\theta(0) = 0$ at $\xi = 0$.

Given that \mathbf{x} is a solution of (see Eq. (D2))

$$\sum_\nu \mathcal{M}_{\mu\nu} \frac{\partial x_\nu}{\partial \xi} \Big|_{\xi=0} = \chi_\mu, \quad (\text{I5})$$

\mathbf{x}' is also a solution of

$$\sum_\nu \mathcal{M}_{\mu\nu} \frac{\partial x'_\nu}{\partial \xi} \Big|_{\xi=0} = \chi_\mu. \quad (\text{I6})$$

Note again that here μ and ν runs through all the elements in \mathbf{x} (Eq. (26)), and we use the variational parameters as the subscripts. Also, we have

$$\frac{\partial x'_\mu}{\partial \xi} \Big|_{\xi=0} = \frac{\partial x_\mu}{\partial \xi} \Big|_{\xi=0} + \sum_s \frac{\partial x_\mu}{\partial \theta_s} \Big|_{\theta=0} \frac{\partial \theta_s}{\partial \xi} \Big|_{\xi=0}. \quad (\text{I7})$$

Consequently, we show that

$$\mathcal{M}_{\mu\nu} \frac{\partial x_\nu}{\partial \theta_s} \Big|_{\theta=0} \frac{\partial \theta_s}{\partial \xi} \Big|_{\xi=0} = 0, \quad (\text{I8})$$

which implies that $\mathcal{M}_{\mu\nu}$ has zero eigenvalues, and the kernels are defined as

$$K_{s,\mu} := \left\{ \frac{\partial x_\mu}{\partial \theta_s} \Big|_{\theta=0} \right\} \quad (\text{I9})$$

such that:

$$M_{\mu\nu} K_{s,\nu} = 0 \quad \forall K_s \in K. \quad (\text{I10})$$

We can fix the gauge by projecting the matrices onto the vector space $v_{i,\mu}$ perpendicular to K , where $v_{i,\mu}$ can be constructed from the Gram-Schmidt process. The reduced fluctuation matrix and the embedding susceptibilities becomes:

$$\bar{\mathcal{M}}_{ij} = v_{i,\mu} \mathcal{M}_{\mu\nu} v_{j,\nu}, \quad (\text{I11})$$

$$\bar{\chi}_{i\mathcal{O}} = v_{i,\mu} \chi_{\mu\mathcal{O}}. \quad (\text{I12})$$

Consequently, we have the physical susceptibility

$$\chi_{\mathcal{O}\mathcal{O}} = \chi_{\mathcal{O}\mathcal{O}}^{(0)} + \bar{\chi}_{i\mathcal{O}} \bar{\mathcal{M}}_{ij}^{-1} \bar{\chi}_{j\mathcal{O}}. \quad (\text{I13})$$

Now the $\bar{\mathcal{M}}_{ij}^{-1}$ does not contain zero modes and the matrix inversion is well defined.

For the model considered in this work, where we restricted the variational variables \mathbf{x} to real numbers (Eqs. (21)-(25)), the $U(1)$ gauge degrees of freedom in the charge, spin, orbital, and spin-orbital channels are fixed. However, we are left with one gauge degree of freedom relating to the Nambu pseudo-spin rotation generator:

$$\mathbf{T} = \tau_1 \otimes \lambda_6 \otimes (i\sigma_y \sigma_z), \quad (\text{I14})$$

where τ_i is the Pauli matrix corresponding to Nambu pseudospin. From the definition of the gauge transformation (Eqs. (H1)-(H3)), we derive the kernel K :

$$\left. \frac{\partial r_s}{\partial \theta} \right|_{\theta=0} = -i \text{Tr}[(\tilde{\mathbf{h}}_s)^\dagger \mathbf{T} \mathbf{R}] = \frac{r_0}{2\sqrt{3}} \delta_{s,P} \quad (\text{I15})$$

$$\left. \frac{\partial l_s}{\partial \theta} \right|_{\theta=0} = -i \text{Tr}[(\mathbf{h}_s)^\dagger [\mathbf{T}, \mathbf{\Lambda}]] = -\frac{l_0}{\sqrt{3}} \delta_{s,P} \quad (\text{I16})$$

$$\left. \frac{\partial d_s}{\partial \theta} \right|_{\theta=0} = i \text{Tr}[(\mathbf{h}_s)^\dagger [\mathbf{T}^t, \mathbf{\Delta}]] = -\frac{d_0}{\sqrt{3}} \delta_{s,P} \quad (\text{I17})$$

$$\left. \frac{\partial D_s}{\partial \theta_j} \right|_{\theta=0} = i \text{Tr}[(\tilde{\mathbf{h}}_s)^\dagger \mathbf{T}^t \mathbf{D}] = \frac{D_0}{2\sqrt{3}} \delta_{s,P} \quad (\text{I18})$$

$$\left. \frac{\partial l_s^c}{\partial \theta} \right|_{\theta=0} = -i \text{Tr}[(\mathbf{h}_s)^\dagger [\mathbf{T}, \mathbf{\Lambda}^c]] = -\frac{l_0^c}{\sqrt{3}} \delta_{s,P}, \quad (\text{I19})$$

where the K vector is only non-zero in the pairing channel. We can then construct the vector space $v_{i,\mu}$ using the Gram-Schmidt process and compute the susceptibilities through Eq. (I11)-(I13).

Appendix J: Validity of the Fermi-liquid approximation

In this section, we show the pairing susceptibility χ^P computed from the equation without enforcing the “quasiparticle constraint” (Eq. (42)) and the equation with the “quasiparticle constraint” (Eq. (56)) in Fig. 9. The χ^P obtained from the two approaches are identical for all the parameter regime, indicating the validity of the Fermi-liquid approximation described in Sec. IV.

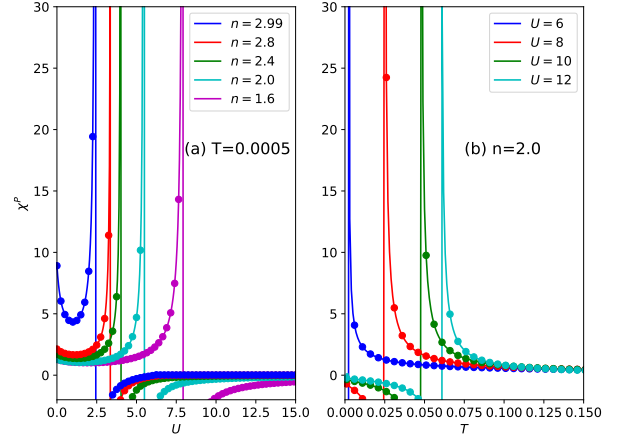


Figure 9. Comparison of the pairing susceptibilities χ^P computed from Eq. (42) (solid line, without “quasiparticle constraint”) and Eq. (56) (filled circles, with “quasiparticle constraint”) for (a) $T = 0.0005$ and $n = 2.99, 2.8, 2.4, 2.0, 1.6$ as a function of U and $J = U/4$, and (b) $n = 2.0$ and $U = 6, 8, 10, 12$ as a function of T and $J = U/4$.

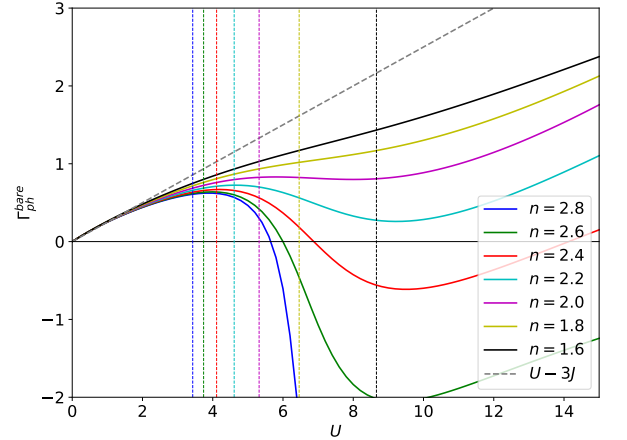


Figure 10. The bare pairing interaction in the particle-hole channel $\Gamma_{\text{ph}}^{\text{bare}}$ (Eq. (K1)) as a function of Coulomb interaction U and $J = U/4$ for filling $n = 2.8, 2.6, 2.4, 2.2, 2.0, 1.8, 1.6$ at temperature $T = 0.0005t$.

Appendix K: Bare pairing interaction in the particle-hole channel

We also compute the bare pairing interaction in the particle-hole channel defined as follows:

$$\Gamma_{\text{ph}}^{\text{bare}} = \frac{1}{4} \left[F_{\text{ch}} + F_{\text{sp}} - F_{\text{orb}} - F_{\text{so}} - \frac{5}{3} F_{\text{orb}^*} - \frac{5}{3} F_{\text{so}^*} \right], \quad (\text{K1})$$

In this case, the summation of the fermionic particle-hole bubbles in Fig. 3 (b) are ignored and only the bare interaction (Landau parameters F_s at $\mathbf{q} = 0$) is considered. Figure 10 shows the bare pairing interaction in the particle-hole channel. We found that the bare pairing

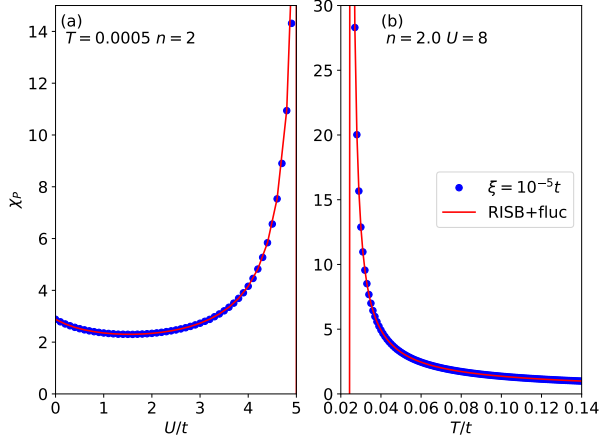


Figure 11. Comparison of the uniform pairing susceptibility $\chi^P(\mathbf{q} = 0, \omega = 0)$ evaluated from fluctuation approach with the pairing susceptibility evaluated from the mean-field solution $\chi^P = \frac{d\langle O_P \rangle}{d\zeta}$ with small pairing field $\zeta = 10^{-5}$ for (a) temperature $T = 0.0005t$ and filling $n = 2.0$. and (b) Coulomb interaction $U = 8t$ and filling $n = 2.0$. We fix the Hund's coupling interaction at $J = U/4$.

interaction only turns negative (signaling the pairing instability) for filling $n < 2.3$.

Appendix L: Consistency check for susceptibility

We perform the consistency check for the pairing susceptibility between the one computed from RISB fluctuation approach and the one computed from RISB mean-field theory with a small pairing field ζ . The definition of the pairing susceptibility in the RISB self-consistent mean-field theory is $\chi^P = \left. \frac{\partial \langle O_P \rangle}{\partial \zeta} \right|_{\zeta \rightarrow 0}$. The results from the two approaches are shown in Fig. 11 (a) as function of Coulomb interaction U for $T = 0.0005t$ and filling $n = 2.0$ and (b) as a function of temperature T for $U = 8t$ and filling $n = 2.0$. We confirm that the $\chi^P(\mathbf{q} = 0, \omega = 0)$ computed from the fluctuation approach (red line) agrees excellently with the χ^P computed from the mean-field theory with a small pairing field $\zeta = 10^{-5}t$ (blue dots). The agreement between the two approaches indicates the consistency of our fluctuation approach within the RISB framework.

Appendix M: Total energy and weak to strong-coupling crossover

We now discuss the energetic of the s -wave spin-triplet pairing state. Figure 12 (a) and (b) shows the kinetic energy gain $\Delta E_k = E_k^N - E_k^{sc}$, the potential energy gain $\Delta E_{\text{pot}} = E_{\text{pot}}^N - E_{\text{pot}}^{sc}$, and the total energy gain $\Delta E_{\text{tot}} = E_{\text{tot}}^N - E_{\text{tot}}^{sc}$ for forming the s -wave spin-triplet

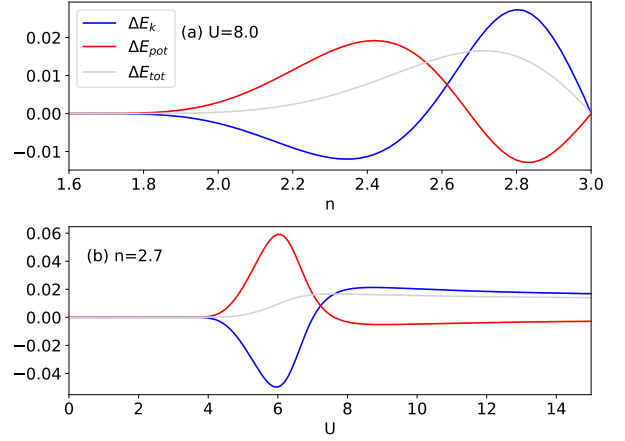


Figure 12. The kinetic energy ΔE_k , the potential energy ΔE_{pot} , and the total energy gain ΔE_{tot} for the superconducting state for (a) at $U = 8t$ and $T = 10^{-4}t$ and (b) as a function of Coulomb interaction U and $J = U/4$ at $n = 2.7$ and $T = 10^{-4}t$.

pairing state, where the superscript N and sc corresponds to the energy in the normal state and the superconducting state, respectively. The energetic in both Fig. (a) and (b) shows a typical weak-coupling to strong-coupling crossover behavior [71, 92, 93], where the energy gain is dominated from the potential energy in the weak-coupling limit, and from the kinetic energy in the strong-coupling limit. Interestingly, we find this crossover locates around the Hund's metal crossover where the quasi-particle weight drops rapidly and the superconducting order parameter shows a pronounce peak.

Appendix N: Application to density matrix embedding theory

In this section, we outline the equations for computing the susceptibility in the “non-interacting bath” DMET (NIB-DMET) formalism. Since the NIB-DMET self-consistent equations can be reproduced from the RISB Lagrangian by enforcing $\mathbf{R} = I$ and an additional constraint in Eq. (44), the formalism in Sec. IV can be directly applied to NIB-DMET by removing the r_s sector of the fluctuation basis in Eq. (45), i.e., no fluctuation in \mathbf{R} . Hence, the NIB-DMET fluctuation basis becomes:

$$\mathbf{x}_{\mathbf{q}} = (l_{\text{ch},\mathbf{q}}, d_{\text{ch},\mathbf{q}}, D_{\text{ch},\mathbf{q}}, l_{\text{ch},\mathbf{q}}^c, \zeta_{\text{ch},\mathbf{q}}, \dots, l_{s,\mathbf{q}}, d_{s,\mathbf{q}}, D_{s,\mathbf{q}}, l_{s,\mathbf{q}}^c, \zeta_{s,\mathbf{q}}, \dots, l_{\text{P},\mathbf{q}}, d_{\text{P},\mathbf{q}}, D_{\text{P},\mathbf{q}}, l_{\text{P},\mathbf{q}}^c, \zeta_{\text{P},\mathbf{q}}), \quad (\text{N1})$$

where, differ from RISB (Eq. (45)), the variables r_s is absent. Following the same derivation in Sec. IV, the NIB-DMET susceptibility of an arbitrary operator \hat{O} has the following form:

$$\chi_{\mathcal{O}\mathcal{O}}(\mathbf{q}) = \chi_{\mathcal{O}\mathcal{O}}^{(0)}(\mathbf{q}) + \sum_{\mu\nu} \chi_{\mu\mathcal{O}}(\mathbf{q}) \mathcal{M}_{\mu\nu}^{-1}(\mathbf{q}) \chi_{\nu\mathcal{O}}(\mathbf{q}), \quad (\text{N2})$$

where the fluctuation matrix \mathcal{M} is given in Appx. E and we have to enforce $\mathbf{R} = I$ in each element. We have also introduced the following susceptibilities:

$$\chi_{\mathcal{O}\mathcal{O}}^{(0)}(\mathbf{q}) = -\frac{T}{2N} \sum_{\omega_n, \mathbf{k}} \text{Tr} \left[\mathbf{G}_{\omega_n, \mathbf{k}+\mathbf{q}} \mathcal{O} \mathbf{G}_{\omega_n, \mathbf{k}} \mathcal{O} \right], \quad (\text{N3})$$

$$\chi_{\mu\mathcal{O}}(\mathbf{q}) = \frac{T}{2N} \sum_{\omega_n, \mathbf{k}} \partial_{x_{\mu, \mathbf{q}}} \text{Tr} \left[\mathbf{G}_{\omega_n, \mathbf{k}+\mathbf{q}, \mathbf{k}}[\xi, \mathbf{x}] \mathcal{O} \right] \Big|_{(\xi=0, \mathbf{x}(\xi=0))}, \quad (\text{N4})$$

where \mathcal{O} is the single-particle matrix representation of a generic operator. The Green's function has the following form:

$$\left[\mathbf{G}_{\omega_n, \mathbf{k}_1, \mathbf{k}_2}[\mathbf{x}, \xi] \right]^{-1} = i\omega_n - \left[H_{\mathbf{k}_1 \mathbf{k}_2}^{\text{qp}} \right]_{ab} + \xi_{\mathbf{k}_1 - \mathbf{k}_2} \left[\mathcal{O} \right]_{ab}, \quad (\text{N5})$$

and $\mathbf{G}_{\omega_n, \mathbf{k}}$ is the Green's function evaluated at $\xi = 0$. We also introduce the quasiparticle Hamiltonian (low-level mean-field Hamiltonian):

$$\left[H_{\mathbf{k}_1 \mathbf{k}_2}^{\text{qp}} \right]_{ab} \equiv \left[\tilde{\epsilon}_{\mathbf{k}_1} \right]_{ab} \delta_{\mathbf{k}_1, \mathbf{k}_2} + \left[\Lambda_{\mathbf{k}_1 - \mathbf{k}_2} \right]_{ab}, \quad (\text{N6})$$

where Λ corresponds to the correlation potential in NIB-DMET.

For the degenerate model considered in this work, the

susceptibility can be written as:

$$\chi_{\mathcal{O}_s \mathcal{O}_s}(\mathbf{q}) = \chi_{\mathcal{O}_s \mathcal{O}_s}^{(0)}(\mathbf{q}) + \chi_{l_s \mathcal{O}_s}(\mathbf{q}) \mathcal{M}_{l_s l_s}^{-1}(\mathbf{q}) \chi_{l_s \mathcal{O}_s}(\mathbf{q}), \quad (\text{N7})$$

where

$$\chi_{l_s \mathcal{O}_s}(\mathbf{q}) = -\frac{T}{2N} \sum_{\omega_n, \mathbf{k}} \text{Tr} \left[\mathbf{G}_{\omega_n, \mathbf{k}+\mathbf{q}} \mathbf{h}_s \mathbf{G}_{\omega_n, \mathbf{k}} \mathbf{h}_s \right] = \chi_{\mathcal{O}_s \mathcal{O}_s}^{(0)}(\mathbf{q}). \quad (\text{N8})$$

$\mathcal{M}_{l_s l_s}^{-1}(\mathbf{q})$ denotes the $\mu = l_s$ and $\nu = l_s$ component of $\mathcal{M}_{\mu\nu}^{-1}(\mathbf{q})$. The $\mathbf{G}_{\omega_n, \mathbf{k}} = [i\omega_n - \tilde{\epsilon}_{\mathbf{k}} - \Lambda]^{-1}$ is the saddle-point Green's function.

Finally, we comment on the advantages and the disadvantages between RISB and NIB-DMET. One advantage of RISB with respect to NIB-DMET is the presence of the renormalization matrix \mathbf{R} . It allows the description of the Mott transition within the single-site approach [94], while in the standard NIB-DMET, one has to use at least a two-site cluster to capture the Mott transition [24]. On the other hand, the additional determination of \mathbf{R} in RISB may require more self-consistency iterations with respect to NI-DMET, leading to more diagonalization of the embedding Hamiltonian \bar{H}_{emb} . Nevertheless, the performance and the accuracy of the two methods are similar [26]. Note that our approach does not apply to the ‘‘interacting bath’’ construction of DMET (IB-DMET), which produces more accurate results than the NIB-DMET [24, 85, 95]. The extension of our approach to IB-DMET will be an interesting future topic.

-
- [1] S E Barnes, *New Method for the Anderson Model*, Journal of Physics F: Metal Physics **6**, 1375–1383 (1976).
- [2] Piers Coleman, *New approach to the mixed-valence problem*, Phys. Rev. B **29**, 3035–3044 (1984).
- [3] Gabriel Kotliar and Andrei E. Ruckenstein, *New Functional Integral Approach to Strongly Correlated Fermi Systems: The Gutzwiller Approximation as a Saddle Point*, Phys. Rev. Lett. **57**, 1362–1365 (1986).
- [4] T. Li, P. Wölfle, and P. J. Hirschfeld, *Spin-Rotation-Invariant Slave-Boson Approach to the Hubbard Model*, Phys. Rev. B **40**, 6817–6821 (1989).
- [5] R Frésard and P. Wölfle, *Unified Slave Boson Representation of Spin and Charge Degrees of Freedom for Strongly Correlated Fermi Systems*, International Journal of Modern Physics B **06**, 685 (1992).
- [6] Serge Florens and Antoine Georges, *Slave-Rotor Mean-Field Theories of Strongly Correlated Systems and the Mott Transition in Finite Dimensions*, Phys. Rev. B **70**, 035114 (2004).
- [7] L. de’Medici, A. Georges, and S. Biermann, *Orbital-Selective Mott Transition in Multiband Systems: Slave-Spin Representation and Dynamical Mean-Field Theory*, Phys. Rev. B **72**, 205124 (2005).
- [8] Antoine Georges, Gabriel Kotliar, Werner Krauth, and Marcelo J. Rozenberg, *Dynamical Mean-Field Theory of Strongly Correlated Fermion Systems and the Limit of Infinite Dimensions*, Rev. Mod. Phys. **68**, 13–125 (1996).
- [9] Frank Lechermann, Antoine Georges, Gabriel Kotliar, and Olivier Parcollet, *Rotationally invariant slave-boson formalism and momentum dependence of the quasiparticle weight*, Phys. Rev. B **76**, 155102 (2007).
- [10] Martin C. Gutzwiller, *Effect of Correlation on the Ferromagnetism of Transition Metals*, Phys. Rev. Lett. **10**, 159–162 (1963).
- [11] J. Büinemann and F. Gebhard, *Equivalence of Gutzwiller and slave-boson mean-field theories for multiband Hubbard models*, Phys. Rev. B **76**, 193104 (2007).
- [12] Christoph Piefke and Frank Lechermann, *LDA + slave-boson approach to the correlated electronic structure of the metamagnetic bilayer ruthenate Sr3Ru2O7*, physica status solidi (b) **248**, 2269–2275 (2011), <https://onlinelibrary.wiley.com/doi/pdf/10.1002/pssb.201147052>.
- [13] Christoph Piefke and Frank Lechermann, *Rigorous Symmetry Adaptation of Multiorbital Rotationally Invariant Slave-Boson Theory with Application to Hund’s Rules Physics*, Phys. Rev. B **97**, 125154 (2018).
- [14] Nicola Lanatà, Yongxin Yao, Xiaoyu Deng, Vladimir Dobrosavljević, and Gabriel Kotliar, *Slave Boson Theory of Orbital Differentiation with Crystal Field Effects: Application to UO2*, Phys. Rev. Lett. **118**, 126401 (2017).

- [15] Nicola Lanatà, Tsung-Han Lee, Yong-Xin Yao, Vladan Stevanović, and Vladimir Dobrosavljević, *Connection between Mott Physics and Crystal Structure in a Series of Transition Metal Binary Compounds*, npj Computational Materials **5**, 30 (2019).
- [16] Luca de' Medici, Jernej Mravlje, and Antoine Georges, *Janus-Faced Influence of Hund's Rule Coupling in Strongly Correlated Materials*, Phys. Rev. Lett. **107**, 256401 (2011).
- [17] Luca de' Medici, Gianluca Giovannetti, and Massimo Capone, *Selective Mott Physics as a Key to Iron Superconductors*, Phys. Rev. Lett. **112**, 177001 (2014).
- [18] Jorge I. Facio, Jernej Mravlje, Leonid Pourovskii, Pablo S. Cornaglia, and V. Vildosola, *Spin-Orbit and Anisotropic Strain Effects on the Electronic Correlations in Sr₂RuO₄*, Phys. Rev. B **98**, 085121 (2018).
- [19] Mark E. Barber, Frank Lechermann, Sergey V. Streltsov, Sergey L. Skornyakov, Sayak Ghosh, B. J. Ramshaw, Naoki Kikugawa, Dmitry A. Sokolov, Andrew P. Mackenzie, Clifford W. Hicks, and I. I. Mazin, *Role of Correlations in Determining the Van Hove Strain in Sr₂RuO₄*, Phys. Rev. B **100**, 245139 (2019).
- [20] Nicola Lanatà, Yong-Xin Yao, Cai-Zhuang Wang, Kai-Ming Ho, Jörg Schmalian, Kristjan Haule, and Gabriel Kotliar, γ - α *Isostructural Transition in Cerium*, Phys. Rev. Lett. **111**, 196801 (2013).
- [21] Nicola Lanatà, Yongxin Yao, Cai-Zhuang Wang, Kai-Ming Ho, and Gabriel Kotliar, *Phase Diagram and Electronic Structure of Praseodymium and Plutonium*, Phys. Rev. X **5**, 011008 (2015).
- [22] Feng Lu, Jianzhou Zhao, Hongming Weng, Zhong Fang, and Xi Dai, *Correlated Topological Insulators with Mixed Valence*, Phys. Rev. Lett. **110**, 096401 (2013).
- [23] G. Kotliar, S. Y. Savrasov, K. Haule, V. S. Oudovenko, O. Parcollet, and C. A. Marianetti, *Electronic Structure Calculations with Dynamical Mean-Field Theory*, Rev. Mod. Phys. **78**, 865–951 (2006).
- [24] Gerald Knizia and Garnet Kin-Lic Chan, *Density Matrix Embedding: A Simple Alternative to Dynamical Mean-Field Theory*, Phys. Rev. Lett. **109**, 186404 (2012).
- [25] Thomas Ayrál, Tsung-Han Lee, and Gabriel Kotliar, *Dynamical Mean-Field Theory, Density-Matrix Embedding Theory, and Rotationally Invariant Slave Bosons: A Unified Perspective*, Phys. Rev. B **96**, 235139 (2017).
- [26] Tsung-Han Lee, Thomas Ayrál, Yong-Xin Yao, Nicola Lanatà, and Gabriel Kotliar, *Rotationally Invariant Slave-Boson and Density Matrix Embedding Theory: Unified Framework and Comparative Study on the One-Dimensional and Two-Dimensional Hubbard Model*, Phys. Rev. B **99**, 115129 (2019).
- [27] Chong Sun, Ushnish Ray, Zhi-Hao Cui, Miles Stoudenmire, Michel Ferrero, and Garnet Kin-Lic Chan, *Finite-temperature density matrix embedding theory*, Phys. Rev. B **101**, 075131 (2020).
- [28] Nicola Lanatà, Xiaoyu Deng, and Gabriel Kotliar, *Finite-temperature Gutzwiller approximation from the time-dependent variational principle*, Phys. Rev. B **92**, 081108 (2015).
- [29] Marco Schiró and Michele Fabrizio, *Time-Dependent Mean Field Theory for Quench Dynamics in Correlated Electron Systems*, Phys. Rev. Lett. **105**, 076401 (2010).
- [30] Joshua S. Kretschmer and Garnet Kin-Lic Chan, *A real-time extension of density matrix embedding theory for non-equilibrium electron dynamics*, The Journal of Chemical Physics **148**, 054108 (2018).
- [31] Hong-Zhou Ye, Henry K. Tran, and Troy Van Voorhis, *Accurate Electronic Excitation Energies in Full-Valence Active Space via Bootstrap Embedding*, Journal of Chemical Theory and Computation **17**, 3335–3347 (2021), pMID: 33957050, <https://doi.org/10.1021/acs.jctc.0c01221>.
- [32] P. V. Sriluckshmy, Max Nusspickel, Edoardo Fertitta, and George H. Booth, *Fully algebraic and self-consistent effective dynamics in a static quantum embedding*, Phys. Rev. B **103**, 085131 (2021).
- [33] Nicola Lanatà, Tsung-Han Lee, Yong-Xin Yao, and Vladimir Dobrosavljević, *Emergent Bloch excitations in Mott matter*, Phys. Rev. B **96**, 195126 (2017).
- [34] D. J. Scalapino, *A common thread: The pairing interaction for unconventional superconductors*, Rev. Mod. Phys. **84**, 1383–1417 (2012).
- [35] N Read and D M News, *On the Solution of the Coqblin-Schrieffer Hamiltonian by the Large-N Expansion Technique*, Journal of Physics C: Solid State Physics **16**, 3273–3295 (1983).
- [36] L. Lilly, A. Muramatsu, and W. Hanke, *Slave-Boson Mean Field Versus Quantum Monte Carlo Results for the Hubbard Model*, Phys. Rev. Lett. **65**, 1379–1382 (1990).
- [37] Th. Jolicoeur and J. C. Le Guillou, *Fluctuations Beyond the Gutzwiller Approximation in the Slave-Boson Approach*, Phys. Rev. B **44**, 2403–2406 (1991).
- [38] M. Lavagna, *Functional-Integral Approach to Strongly Correlated Fermi Systems: Quantum Fluctuations Beyond the Gutzwiller Approximation*, Phys. Rev. B **41**, 142–148 (1990).
- [39] T. Li, Y. S. Sun, and P. Wölfle, *Dynamic Response Functions of Hubbard Model in Gutzwiller Approximation*, Zeitschrift für Physik B Condensed Matter **82**, 369–374 (1991).
- [40] E. Arrigoni and G. C. Strinati, *Exact Criterion for Choosing the Hopping Operator in the Four-Slave-Boson Approach*, Phys. Rev. B **52**, 13707–13710 (1995).
- [41] R. Raimondi and C. Castellani, *Lower and Upper Hubbard Bands: A Slave-Boson Treatment*, Phys. Rev. B **48**, 11453–11456 (1993).
- [42] Walter Zimmermann, Raymond Frésard, and Peter Wölfle, *Spin and Charge Structure Factor of the Two-Dimensional Hubbard Model*, Phys. Rev. B **56**, 10097–10104 (1997).
- [43] Vu Hung Dao and Raymond Frésard, *Collective Modes in the Paramagnetic Phase of the Hubbard Model*, Phys. Rev. B **95**, 165127 (2017).
- [44] David Riegler, Michael Klett, Titus Neupert, Ronny Thomale, and Peter Wölfle, *Slave-Boson Analysis of the Two-Dimensional Hubbard Model*, Phys. Rev. B **101**, 235137 (2020).
- [45] G. Seibold and J. Lorenzana, *Time-Dependent Gutzwiller Approximation for the Hubbard Model*, Phys. Rev. Lett. **86**, 2605–2608 (2001).
- [46] G. Seibold, F. Becca, P. Rubin, and J. Lorenzana, *Time-dependent Gutzwiller Theory of Magnetic Excitations in the Hubbard Model*, Phys. Rev. B **69**, 155113 (2004).
- [47] Michele Fabrizio, *Quantum Fluctuations Beyond the Gutzwiller Approximation*, Phys. Rev. B **95**, 075156 (2017).
- [48] G. Seibold, F. Becca, and J. Lorenzana, *Theory of Antibound States in Partially Filled Narrow Band Systems*, Phys. Rev. Lett. **100**, 016405 (2008).

- [49] G. Seibold, F. Becca, and J. Lorenzana, *Time-dependent Gutzwiller Theory of Pairing Fluctuations in the Hubbard Model*, Phys. Rev. B **78**, 045114 (2008).
- [50] E von Oelsen, G Seibold, and J Büemann, *Time-Dependent Gutzwiller Theory for Multi-band Hubbard Models*, New Journal of Physics **13**, 113031 (2011).
- [51] E. v. Oelsen, G. Seibold, and J. Büemann, *Time-Dependent Gutzwiller Theory for Multiband Hubbard Models*, Phys. Rev. Lett. **107**, 076402 (2011).
- [52] Philipp Werner, Emanuel Gull, Matthias Troyer, and Andrew J. Millis, *Spin Freezing Transition and Non-Fermi-Liquid Self-Energy in a Three-Orbital Model*, Phys. Rev. Lett. **101**, 166405 (2008).
- [53] Shintaro Hoshino and Philipp Werner, *Superconductivity from Emerging Magnetic Moments*, Phys. Rev. Lett. **115**, 247001 (2015).
- [54] M Zegrodnik, J Spalek, and J Büemann, *Coexistence of Spin-Triplet Superconductivity with Magnetism within a Single Mechanism for Orbital Degenerate Correlated Electrons: Statistically Consistent Gutzwiller Approximation*, New Journal of Physics **15**, 073050 (2013).
- [55] M Zegrodnik, J Büemann, and J Spalek, *Even-Parity Spin-Triplet Pairing by Purely Repulsive Interactions for Orbital Degenerate Correlated Fermions*, New Journal of Physics **16**, 033001 (2014).
- [56] M. Capone, M. Fabrizio, C. Castellani, and E. Tosatti, *Strongly Correlated Superconductivity*, Science **296**, 2364–2366 (2002).
- [57] Massimo Capone, Michele Fabrizio, and Erio Tosatti, *Direct Transition between a Singlet Mott Insulator and a Superconductor*, Phys. Rev. Lett. **86**, 5361–5364 (2001).
- [58] Junjiro Kanamori, *Electron Correlation and Ferromagnetism of Transition Metals*, Progress of Theoretical Physics **30**, 275–289 (1963).
- [59] Alfred K. C. Cheung and D. F. Agterberg, *Superconductivity in the Presence of Spin-Orbit Interactions Stabilized by Hund Coupling*, Phys. Rev. B **99**, 024516 (2019).
- [60] Han Gyeol Suh, Henri Menke, P. M. R. Brydon, Carsten Timm, Aline Ramires, and Daniel F. Agterberg, *Stabilizing Even-Parity Chiral Superconductivity in Sr₂RuO₄*, Phys. Rev. Research **2**, 032023(R) (2020).
- [61] S.-O. Kaba and D. Sénéchal, *Group-Theoretical Classification of Superconducting States of Strontium Ruthenate*, Phys. Rev. B **100**, 214507 (2019).
- [62] A. Isidori and M. Capone, *Rotationally Invariant Slave Bosons for Strongly Correlated Superconductors*, Phys. Rev. B **80**, 115120 (2009).
- [63] Gabriel Kotliar and Jialin Liu, *Superconducting Instabilities in the Large- U Limit of a Generalized Hubbard Model*, Phys. Rev. Lett. **61**, 1784–1787 (1988).
- [64] Marco Grilli and Gabriel Kotliar, *Fermi-Liquid Parameters and Superconducting Instabilities of a Generalized t - J Model*, Phys. Rev. Lett. **64**, 1170–1173 (1990).
- [65] M. Grilli, R. Raimondi, C. Castellani, C. Di Castro, and G. Kotliar, *Superconductivity, Phase Separation, and Charge-Transfer Instability in the $U=\infty$ Limit of the Three-Band Model of the CuO₂ Planes*, Phys. Rev. Lett. **67**, 259–262 (1991).
- [66] A. Sudbø and A. Houghton, *Charge Fluctuations: Spin Fluctuations and Superconductivity in a CuO₂ Sheet*, Phys. Rev. B **42**, 4105–4116 (1990).
- [67] Antoine Georges, Luca de’ Medici, and Jernej Mravlje, *Strong Correlations from Hund’s Coupling*, Annual Review of Condensed Matter Physics **4**, 137–178 (2013).
- [68] Aldo Isidori, Maja Berović, Laura Fanfarillo, Luca de’ Medici, Michele Fabrizio, and Massimo Capone, *Charge Disproportionation, Mixed Valence, and Janus Effect in Multiorbital Systems: A Tale of Two Insulators*, Phys. Rev. Lett. **122**, 186401 (2019).
- [69] J. E. Han, *Spin-Triplet s -wave Local Pairing Induced by Hund’s Rule Coupling*, Phys. Rev. B **70**, 054513 (2004).
- [70] Walter Metzner and Dieter Vollhardt, *Correlated Lattice Fermions in $d = \infty$ Dimensions*, Phys. Rev. Lett. **62**, 324–327 (1989).
- [71] M Bak and R Micnas, *Superconducting Properties of the Attractive Hubbard Model in the Slave-Boson Approach*, Journal of Physics: Condensed Matter **10**, 9029–9054 (1998).
- [72] Luca de’ Medici, *Hund’s Induced Fermi-Liquid Instabilities and Enhanced Quasiparticle Interactions*, Phys. Rev. Lett. **118**, 167003 (2017).
- [73] Christoph M. Puetter and Hae-Young Kee, *Identifying Spin-Triplet Pairing in Spin-Orbit Coupled Multi-Band Superconductors*, EPL (Europhysics Letters) **98**, 27010 (2012).
- [74] Austin W. Lindquist and Hae-Young Kee, *Distinct Reduction of Knight Shift in Superconducting State of Sr₂RuO₄ under Uniaxial Strain*, Phys. Rev. Research **2**, 032055(R) (2020).
- [75] Jonathan Clepkens, Austin W. Lindquist, and Hae-Young Kee, *Shadowed Triplet Pairings in Hund’s Metals with Spin-Orbit Coupling*, arXiv:2009.08597 (2020).
- [76] Oskar Vafeek and Andrey V. Chubukov, *Hund Interaction, Spin-Orbit Coupling, and the Mechanism of Superconductivity in Strongly Hole-Doped Iron Pnictides*, Phys. Rev. Lett. **118**, 087003 (2017).
- [77] Piers Coleman, Yashar Komijani, and Elio J. König, *Triplet Resonating Valence Bond State and Superconductivity in Hund’s Metals*, Phys. Rev. Lett. **125**, 077001 (2020).
- [78] S. Raghu, Xiao-Liang Qi, C. Honerkamp, and Shou-Cheng Zhang, *Topological Mott Insulators*, Phys. Rev. Lett. **100**, 156401 (2008).
- [79] Maxim Dzero, Kai Sun, Victor Galitski, and Piers Coleman, *Topological Kondo Insulators*, Phys. Rev. Lett. **104**, 106408 (2010).
- [80] Michael Klett, Seulgi Ok, David Riegler, Peter Wölfle, Ronny Thomale, and Titus Neupert, *Topology and magnetism in the Kondo insulator phase diagram*, Phys. Rev. B **101**, 161112 (2020).
- [81] Peng Zhang, Koichiro Yaji, Takahiro Hashimoto, Yuichi Ota, Takeshi Kondo, Kozo Okazaki, Zhijun Wang, Jinsheng Wen, G. D. Gu, Hong Ding, and Shik Shin, *Observation of topological superconductivity on the surface of an iron-based superconductor*, Science **360**, 182–186 (2018).
- [82] Wenyao Liu, Lu Cao, Shiyu Zhu, Lingyuan Kong, Guangwei Wang, Michal Papaj, Peng Zhang, Ya-Bin Liu, Hui Chen, Geng Li, Fazhi Yang, Takeshi Kondo, Shixuan Du, Guang-Han Cao, Shik Shin, Liang Fu, Zhiping Yin, Hong-Jun Gao, and Hong Ding, *A new Majorana platform in an Fe-As bilayer superconductor*, Nature Communications **11**, 5688 (2020).
- [83] G. Rohringer, H. Hafermann, A. Toschi, A. A. Katanin, A. E. Antipov, M. I. Katsnelson, A. I. Lichtenstein, A. N. Rubtsov, and K. Held, *Diagrammatic Routes to Nonlocal Correlations Beyond Dynamical Mean Field Theory*, Rev. Mod. Phys. **90**, 025003 (2018).

- [84] Bruno Senjean, Naoki Nakatani, Masahisa Tsuchiizu, and Emmanuel Fromager, *Site-occupation embedding theory using Bethe ansatz local density approximations*, Phys. Rev. B **97**, 235105 (2018).
- [85] Ireneusz W. Bulik, Gustavo E. Scuseria, and Jorge Dukelsky, *Density matrix embedding from broken symmetry lattice mean fields*, Phys. Rev. B **89**, 035140 (2014).
- [86] Sajanathan Sekaran, Masahisa Tsuchiizu, Matthieu SaubanÅšre, and Emmanuel Fromager, *Householder transformed density matrix functional embedding theory*, (2021), arXiv:2103.04194 [cond-mat.str-el].
- [87] Michele Fabrizio, *Gutzwiller Description of Non-Magnetic Mott Insulators: Dimer Lattice Model*, Phys. Rev. B **76**, 165110 (2007).
- [88] Nicola Lanatà, Paolo Barone, and Michele Fabrizio, *Superconductivity in the Doped Bilayer Hubbard Model*, Phys. Rev. B **80**, 224524 (2009).
- [89] Nicola Lanatà, Hugo U. R. Strand, Xi Dai, and Bo Hellsing, *Efficient Implementation of the Gutzwiller Variational Method*, Phys. Rev. B **85**, 035133 (2012).
- [90] John Rogers, Tsung-Han Lee, Sahar Pakdel, Wenhui Xu, Vladimir Dobrosavljević, Yong-Xin Yao, Ove Christensen, and Nicola Lanatà, *Bypassing the computational bottleneck of quantum-embedding theories for strong electron correlations with machine learning*, Phys. Rev. Research **3**, 013101 (2021).
- [91] Bo-Xiao Zheng, Chia-Min Chung, Philippe Corboz, Georg Ehlers, Ming-Pu Qin, Reinhard M. Noack, Hao Shi, Steven R. White, Shiwei Zhang, and Garnet Kin-Lic Chan, *Stripe order in the underdoped region of the two-dimensional Hubbard model*, Science **358**, 1155–1160 (2017).
- [92] J. O. Sofo and C. A. Balseiro, *Slave-Boson Mean-Field Theory for the Negative-U Hubbard Model*, Phys. Rev. B **45**, 377–382 (1992).
- [93] Bogdan R. Bulka and Stanislaw Robaszkiewicz, *Superconducting Properties of the Attractive Hubbard Model: A Slave-Boson Study*, Phys. Rev. B **54**, 13138–13151 (1996).
- [94] W. F. Brinkman and T. M. Rice, *Application of Gutzwiller's Variational Method to the Metal-Insulator Transition*, Phys. Rev. B **2**, 4302–4304 (1970).
- [95] Masataka Kawano and Chisa Hotta, *Comparative study of the density matrix embedding theory for Hubbard models*, Phys. Rev. B **102**, 235111 (2020).